Physics – Uspekhi **53** (9) 863 – 892 (2010)

REVIEWS OF TOPICAL PROBLEMS PACS numbers: 73.63.Fg, 85.35.Kt, 85.45.Db

Carbon nanotube-based electron field emitters

A V Eletskii

DOI: 10.3367/UFNe.0180.201009a.0897

Contents

Abstract. The current status of research and development of carbon nanotubes (CNTs) electron field emitters is reviewed. The physical aspects of electron field emission that underlie the unique emission properties of CNTs are considered. Physical effects and phenomena affecting the emission characteristics of CNT cathodes are analyzed. Effects given particular attention include the electric field enhancement near a CNT tip; electric field screening by neighboring nanotubes; statistical spread of the parameters of the individual CNTs comprising the cathode; the effects of heat leading to thermal degradation of nanotubes during emission, and adsorbate effects on the surface of the emitter. Advances in vacuum electronics due to the use of CNT field cathodes are reviewed.

1. Introduction

Carbon nanotubes (CNTs) are elongated cylindrical structures ranging between one and several dozen nanometers in diameter and up to several micrometers in length and consisting of one or several hexagonal graphitic layers rolled into a tube. The end of a nanotube is usually a hemispherical cap that can be considered as half of a fullerene molecule. However, as distinct from fullerenes which are a molecular modification of carbon, CNTs comprise the properties of both molecular object and condensed phase, and therefore can be considered as an intermediate state of a substance between these two forms. This peculiarity is attracting the increasing interest of researchers whose activity is directed at investigating basic properties of such exotic objects under various conditions. During the last several years there has been a real boom in studies addressed at producing, establishing the physical and chemical characteristics of, and determining the most effective applications of CNTs. Thousands of articles are released annually on this subject, resulting in a quick change of our notions on the mechanisms of the synthesis of CNTs under various experimental conditions, their structural, physical, and chemical properties, and opportunities for their applied usage. For this reason, particularly, the review article by the author on the emission properties of CNTs [1], published in *Physics–Uspekhi* more than 8 years ago, is now rather dated and is mainly of historical interest.

It is usually believed that CNTs were discovered by Sumio Iijima in 1991 [2], while elongated carbon structures a nanometer in diameter were observed and described by various authors [3–5] well before this publication. CNTs represent a very attractive subject for nanotechnologies due to the fortunate combination of miniature size, good electric conductivity, and high mechanical, chemical, and thermal stability. The high sorption ability of CNTs allows one to consider them as a potential means of storing various gaseous, liquid and solid substances, protecting them from external influences [6]. The unique mechanical characteristics of CNTs and specifically recordable magnitude of the elastic modulus reaching the TPa level [7] make this object a potential base of a new type of materials combining enhanced hardness with electric conductivity and thermal and chemical stability. The production methods of CNTs, their physical and chemical properties, and some potential applications have been reviewed in detail in many monographs and articles (see Refs [1, 7–13] and the literature cited therein).

An important peculiarity of CNTs is their high aspect ratio (ratio of height to diameter). Due to this feature, the

A V Eletskii Russian Research Centre 'Kurchatov Institute',
pl. Kurchatova 1, 123182 Moscow, Russian Federation
Tel./Fax (7-499) 196 99 78
E-mail: eletskii@imp.kiae.ru

Received 19 March 2010, revised 19 April 2010
Uspekhi Fizicheskikh Nauk **180** (9) 897 – 930 (2010)
DOI: 10.3367/UFNr.0180.201009a.0897
Translated by A V Eletskii; edited by A Radzig

electric field strength in the vicinity of the nanotube's tip can exceed by hundreds of times the relevant average value of this parameter determined by an external source. This peculiarity, in turn, manifests itself in the possibility of obtaining a quite high electron field emission current from CNTs at a moderate magnitude of the applied voltage [14–20]. Due to this, CNT-based electron field emitters far exceed other types of electron field emission cathodes in their emission characteristics, attracting considerable interest from many developers of new types of vacuum electronic devices. Among these devices should be listed first of all flat panel displays [21–23], cathode ray tubes [24], X-ray sources [25–27], and microwave radiation sources and amplifiers [28, 29]. The development of CNT-based electron field emitters has promoted the creation of a new class of electrovacuum devices distinguished by a small lateral size and moderate supply voltage. The present article reviews the current status of investigations addressed at establishing the emission ability of CNTs and cathodes based on them, as well as the development of relevant electrovacuum devices containing such cathodes. The physical principles forming the basis of the operation of CNT-based electron field emitters are described. The natural limitations on their operational characteristics, related to the electric field screening effects in CNT arrays, are analyzed as are the space charge and thermal effects, and statistical spread in parameters of individual nanotubes making up the array. Recent advances in the development of specific devices containing CNT-based cathodes are considered. Note that the problems related to the development of CNT-based electron field emitters have been reviewed briefly in Refs [30–32].

2. Emission properties of an individual nanotube

2.1 Electron field emission and the Fowler–Nordheim equation

The phenomenon of electron field emission is based on the effect of quantum tunneling of electrons found inside a ground conductor through a barrier that is formed by the ionic lattice of the conductor and the external electric field [33]. A simple quantum-mechanical approach [33] results in the following dependence of the emission current density J on the electric field strength E, called the Fowler–Nordheim (FN) equation:

$$J = C_1 E^2 \exp\left(-\frac{C_2}{E}\right). \tag{1}$$

Here, the parameters C_1 and C_2 are expressed through the electron work function φ for the conductor under consideration and the fundamental constants (the charge e and the mass m of electron, and the Planck constant h):

$$C_1 = \frac{e^3}{8\pi h t^2(y)\varphi}, \qquad C_2 = \frac{8\pi\sqrt{2m}}{3he}\,\varphi^{3/2}\theta(y), \qquad y = \frac{e(eE)^{1/2}}{\varphi}. \tag{2}$$

The functions $t(y)$ and $\theta(y)$ constitute smoothly changing dependences that can be well approximated by the relations $t(y) \approx 1$ and $\theta(y) \approx 1 - y^2$. The total emission current I is determined by the integration of equation (1) over the emitting surface:

$$I = \int_S J\,\mathrm{d}S.$$

The Fowler–Nordheim equation (1) has an approximate character. This relation corresponds to the 1D situation, when the emitting surface of a conductor is an infinite plane oriented perpendicular to the direction of the external electric field. Moreover, this relation has been derived assuming that all the conduction electrons in the emitter have a similar energy corresponding to the Fermi level of the material. This assumption is equivalent to the supposition that the temperature of the conductor is negligibly small compared with the Fermi level (or the work function φ). In the case of violation of this supposition, the energy of electrons capable of emissions can be different, which results in a temperature dependence of the emission current that can be taken into account using the relevant correction to the FN equation [34, 35]. In addition, it is assumed that the electron work function of the emitter does not depend on the orientation of the electric field relative to the crystal axes of the conductor. Apparently, the validity of this assumption with respect to carbon nanotubes has not yet been studied. However, the spread in the measured values [1] of the electron work function for CNTs produced in different conditions and possessing various structures indicates the existence of such dependence.

One more factor complicating the character of the dependence (1) is the Shottky effect which manifests itself in a lowering of the potential barrier formed by the external electric field due to the interaction of the electron escaping from the surface of the emitter with its mirror reflection. This effect is accounted for by the correcting function $\theta(y)$ entering into expression (2), which is notable in strong fields. In the case of CNTs, whose electron work function is about $\varphi \approx 5$ eV, this correction is significant at the electric field strength of the order of or higher than 10^8 V cm^{-1}. Usually, the value of this correction is within the uncertainty related to such factors as structural defects in CNTs disturbing their electron characteristics, the dependence of the work function on the orientation of the CNT, etc. These factors will be considered in detail below.

It should be noted that the Fowler–Nordheim equation (1) relates to plane geometry conductors. In this case, the electron emission problem is 1D. The real emitters, and specifically CNTs, are characterized by a considerably more complex structure. A nanotube promotes a significant distortion of the electric field in the vicinity of its tip. Moreover, the strengths of the electric field acting on various areas of the tip differ from each other. In this connection there arises the problem of evaluation of the emission current of a CNT as a function of the applied voltage, taking into account the real geometry of the emitter and real distribution of the electric field in its vicinity. This problem has been formulated by many authors (see, e.g., Refs [36–44] and the references cited therein). Such calculations promote a deeper understanding of the mechanism of the electron field emission from CNTs. However, one should note that the degree of uncertainty of the geometry of both the electric field and the CNTs composing the emitter array, the dependence of emission characteristics on the sort and number of adsorbed molecules, and the considerable uncontrollable spread in the electronic properties of CNTs promote an uncertainty in their emission characteristics. This uncertainty falls outside the

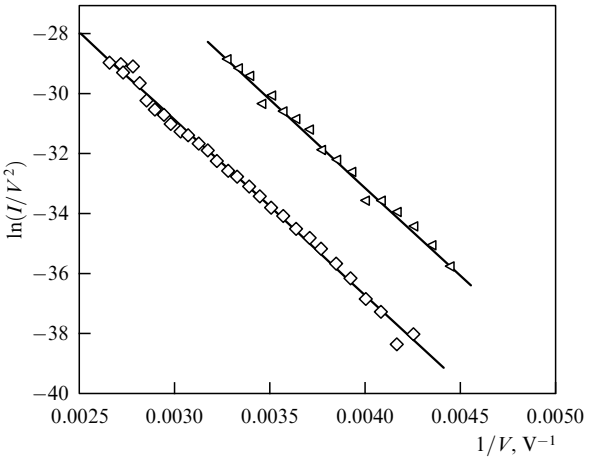

Figure 1. Typical current–voltage characteristics of an individual emitter on the basis of a multiwalled nanotube 8 nm in diameter and 1.1 μm in length, measured before (triangles) and after (rhombi) thermal treatment [45].

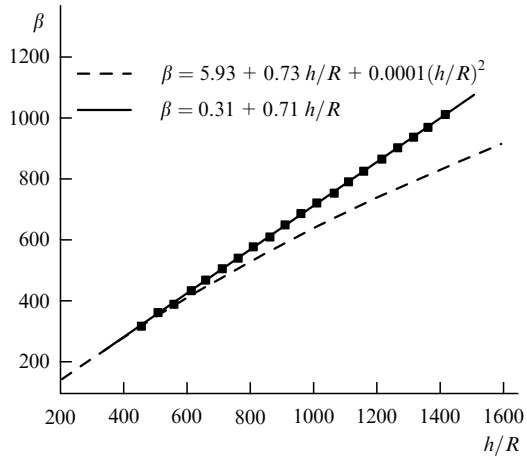

Figure 2. Dependence of the electric field amplification factor on the aspect ratio of a nanotube. Solid line: the nanotube is modeled by a conductive cylinder with a flat cap [46]; broken line: the nanotube is modeled by stacked identical conducting spheres [47]; R is the CNT radius.

limits of corrections to the FN equation (1) related to the above-cited approaches. This can be seen, in particular, from the current–voltage $(I-V)$ characteristics of an individual CNT (Fig. 1) that are in a good agreement with relation (1) within a wide range of the emission current. Such an agreement allows one to utilize equation (1) as a quite convenient starting point for analysis of experimental data concerning CNT-based electron field emitters. The physical mechanisms causing notable violation of this relation will be analyzed in detail below.

A convenient way to treat and analyze experimental data on the basis of FN equation (1) consists in a logarithmic representation of this relation, which results in a directly proportional dependence between the logarithm of a ratio J/E^2 (or I/E^2) and an inverse electric field strength $1/E$:

$$\ln\left(\frac{J}{E^2}\right) = C_1 - \frac{C_2}{E}\,. \tag{3}$$

The rectilinear shape of this dependence indicates the mechanism of the electron emission relating to the electron field emission effect. The parameters of this dependence, such as its slope and the points of crossing with the axes permit, in principle, determining the area of the emitting surface and the electron work function.

The results of numerous experiments imply that the emission properties of an individual CNT are described quite well by FN equation (1). This is illustrated by the current–voltage characteristics of an individual CNT, measured in Ref. [45] by means of a field emission scanning electron microscope (FESEM) before and after its thermal treatment (see Fig. 1). As is seen, even though FN equation (1) is rather approximate, the current–voltage characteristics have a linear shape within a quite wide region of variability of the applied voltage. Therefore, this equation describes experimental data rather well. Possible deviations of measured current–voltage characteristics from the FN equation are always reasoned physically, which will be analyzed in detail below.

2.2 Electric field amplification

The most important peculiarity of carbon nanotubes in terms of their emission properties is a high aspect ratio (the ratio of the length h to the diameter d). Due to this peculiarity, the magnitude of the electric field strength E in the vicinity of the tip of a vertically aligned individual nanotube is many times higher than the average value E_0 of this parameter, defined as the ratio of the applied voltage U to the distance D between the nanotube's tip and the anode. The ability of an emitter to enhance the electric field is characterized by the field amplification factor β, which is defined as the ratio of the real magnitude of the electric field strength E to the average value E_0:

$$\beta = \frac{E}{E_0} = \frac{ED}{U}\,. \tag{4}$$

Since the value of the aspect ratio for CNTs can reach 10^3 and even higher, the electron field emission of nanotubes occurs at much lower values of the applied voltage than in the case of conventional electron field emitters. This offers an opportunity for the development of a new generation of electrovacuum devices distinguished by a lower level of the applied voltage and power consumption. The dependence of the electric field amplification factor on the geometry of the nanotube and interelectrode gap can be evaluated on the basis of the solution to the electrostatic problem, which is reduced to the solution of the Laplace equation for the vicinity of a ground CNT with the boundary conditions corresponding to zero potential on the cathode surface and a fixed value of the potential on the anode surface. The numerical calculations allow the determination of the electric field strength within the gap space and, therefore, the evaluation of the field amplification factor according to Eqn (4). An example of such a calculation is shown in Fig. 2 presenting the dependences of the field amplification factor β on the nanotube's aspect ratio, evaluated in Refs [46, 47]. The nanotube was modeled by a vertically aligned cylinder ending with a flat cap [46], and by a column consisting of stacked conducting spheres [47]. As is seen, the aspect ratio dependence of the field amplification factor is close to the linear one:

$$\beta \approx \frac{h}{d}\,. \tag{5}$$

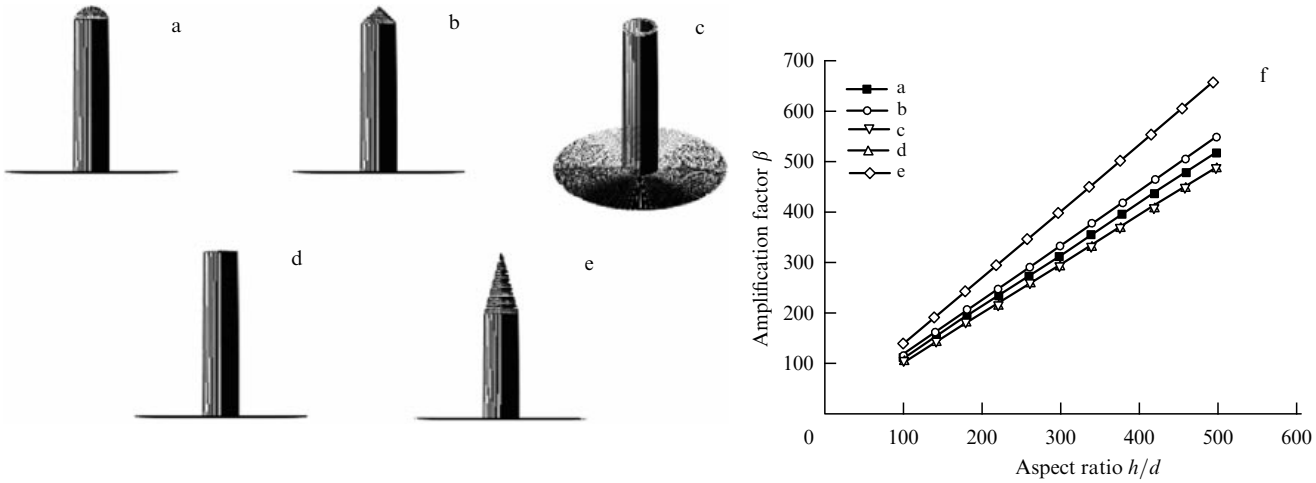

Figure 3. Various types of CNT tips used for calculating the dependence of the electric field amplification factor on the aspect ratio: (a) hemisphere; (b) cone with the vertex angle of 90°; (c) open hollow tube 1 nm thick; (d) flat cap; (e) cone with the vertex angle of 30°, and (f) the results of calculations performed for a nanotube 10 nm in diameter and of variable length. The interelectrode gap is 200 μm, and the applied voltage is 1000 V [48].

At high aspect ratios one can see that some distinction in the behavior of these dependences obtained within the framework of various models is revealed, which can be explained by different approaches to modeling CNTs.

The degree of sensitivity of the field amplification factor of a nanotube, β, to the structure of its end can be estimated on the basis of computations of the aspect ratio dependences of this factor performed for nanotubes with various tip structures [48]. The calculations were done for an individual nanotube 10 nm in diameter and of various heights. The inter-electrode spacing was set to 200 μm, and the applied voltage to 1000 V. Figures 3a–e demonstrate five types of tips for which the calculations were performed: (a) hemisphere; (b) cone with a vertex angle of 90°; (c) open hollow cylinder with a wall 1 nm in thickness; (d) flat cap, and (e) cone with a vertex angle of 30°. The calculated results are given in Fig. 3f. As is seen, a change in the tip structure results in a corresponding variation in the field amplification factor within the range of 5–7%. A notably higher value of the field amplification factor is observed for a conical cap with a cone angle of 30°. In this case, the tip's structure produces an additional field amplification effect.

The above-cited calculations were performed assuming that the interelectrode distance D considerably exceeds the nanotube's height h. If this assumption is violated the factor β should depend not only on the aspect ratio of the nanotube but also on the ratio h/D. Thus, if a nanotube with a flat cap is spaced from the anode surface by a distance D which is much shorter than the nanotube's diameter d, the nanotube and the anode surface can be treated as a flat capacitor. Then, the electric field strength E_1 in the space under consideration is expressed as $E_1 = U/D$. Since the average magnitude of the electric field strength in the gap is $E_0 = U/(h + D)$, the field amplification factor β is given by the following relation

$$\beta = \frac{E_1}{E_0} = \frac{U(h+D)}{DU} \approx \frac{h+D}{D} . \tag{6}$$

As is seen in the limiting case $D \ll d$, the field amplification factor does not depend on the nanotube's diameter and is only determined by the ratio between the nanotube's height and the interelectrode spacing. In the general case, at an arbitrary relationship between the parameters D and d, the field amplification factor naturally depends on the inter-electrode spacing in a more complicated manner, and this dependence also contains as a parameter the nanotube's diameter. One can propose the following interpolation formula that expresses the field amplification factor through geometric parameters of the system at an arbitrary relationship between the quantities h, d, and D [49]:

$$\beta = \frac{h}{d}\left(1 + \frac{d}{D}\right) . \tag{7}$$

This expression transforms into Eqns (5) and (6) in the limiting cases corresponding to the inequalities $D \gg d$ and $D \ll d$, respectively.

The dependence of the β factor on the geometric parameters of a cathode at short interelectrode spacings was studied both experimentally and theoretically by the authors of Refs [50, 51], who measured the field amplification factor by means of a specially designed device. In this device, a sharp tungsten tip etched by the electrochemical method was used as a cathode moved with respect to an anode by means of a piezomanipulator. A gold wire with a spherical cap was utilized as an anode. The device was introduced inside the vacuum chamber of a transmission electron microscope (TEM). The field amplification factor was evaluated by treating the current–voltage characteristics of the emitter represented in the FN coordinates. The results of such a treatment are in qualitative agreement with the above-performed estimations and are confirmed by the results of more comprehensive electrostatic calculations [50, 51]. The calculations were performed for vertically aligned CNTs 40 nm in diameter and with $h = 1$, 2, and 3 μm in height, which corresponds to the aspect ratio $\alpha = h/d = 25$, 50, and 75, respectively. The applied voltage U was set to 100 V. The computations indicate that the dependence of the field amplification factor β on the interelectrode distance D manifests itself for $D/h < 5$, while at $D \sim h$ the field amplification factor exceeds by about two times the asymptotic magnitude inherent to wide gaps. The numerically calculated results are well approximated by the following expression

$$\beta = \frac{h}{d}\left[0.9 + 1.07\left(\frac{d}{D}\right)^{0.42}\right] . \tag{8}$$

However, this equation does not have the correct asymptotic form as $D \ll d$.

In order to avoid misunderstanding, one should note a difference in the definition of the field amplification factor introduced by various authors. The standard approach [1], expressed by Eqn (1), defines the field amplification factor as the ratio of the electric field strength in the vicinity of the CNT to the relevant magnitude in the gap in the absence of a nanotube. The alternative approach [50–53] defines this parameter as the ratio of the electric field strength in the vicinity of the CNT to the relevant value at an anode surface. These two definitions result in the same magnitudes of β for wide interelectrode gaps $D \gg h$. However, upon violation of this inequality, the magnitudes of the field amplification factor calculated using two these definitions notably differ. Thus, the alternative definition for $d \gg D$ results in a paradox conclusion on the absence of the field amplification effect ($\beta = 1$). Naturally, the magnitudes of the electric field strength in the vicinity of a nanotube tip, evaluated on the basis of the two above definitions of the field amplification factor, coincide; therefore, the alternative definition of the field amplification factor should be treated as inconvenient and hindering the analysis, but not as incorrect.

2.3 Structural defects

Defects disturbing the structure of CNTs can affect their emission ability. Among all the possible structural defects in CNTs, one should first note two: vacancy defects that manifest themselves in the form of vacancies in the hexagonal lattice of a nanotube, and Stone–Wells defects which can be considered as the result of substituting a heptagon–pentagon pair for a pair of hexagons. The influence of these two types of defects on the emission properties of a CNT was studied theoretically in Ref. [54] using the density functional theory (DFT). The results of this work indicate that structural defects form scattering centers breaking the ballistic character of transport in CNTs. The influence of defects on the emission properties of a CNT is represented by the factor k_d in the FN equation. The dependences of this factor on the number of defects of various types are presented in Fig. 4 [54]. As is seen, defects of various types have different influences on the emission properties of CNTs. While the Stone–Wells defects lower the emission current due to breaking the ballistic character of transport in CNTs, the occurrence of vacancy defects, on the contrary, promotes an increase in the emission current. The latter is caused by the formation of additional electronic states in the electron structure of the CNT, for which the electron work function is lower than in the case of an ideal nanotube.

2.4 Adsorbates

Well reproducible current–voltage characteristics of a CNT-based emitter can be obtained only if the nanotube's surface is not covered by adsorbed molecules and radicals. Otherwise, the ohmic heating of the nanotube will promote the thermal desorption of such molecules, which results in a change in the electronic properties during the emission. This phenomenon is well recognized for conventional metal-based emission cathodes. Indeed, it has been stated [55, 56], that the room-temperature emission properties of the cathode are determined by surface contaminations if this surface is not subjected to the procedure of thorough cleaning. Thus, the occurrence of adsorbates may have both a positive and a negative effect on the emission characteristics of an emitter.

The influence of adsorbates on the emission properties of CNTs was first revealed in Refs [57–59], the authors of which observed three different modes of field emission from single-layer nanotubes within the temperature range between 300 and 1800 K. The first mode (I) is observed within the temperature range between 300 and 900 K and corresponds to the availability of adsorbates on the nanotube's surface. The second mode (II) occurs at enhanced temperatures when the main part of adsorbed molecules and radicals is removed as a result of thermal action. Mode II passes to mode III at temperatures exceeding 1600 K. This passage is accompanied by an abrupt decrease in the emission current for all the nanotubes. The transition temperature is proportional to the applied voltage, so the electric field stabilizes the emission from the cathode.

Single-walled nanotubes between 0.7 and 1.2 nm in diameter were produced by the electric arc method with the use of Fe and Ni catalysts. Besides CNTs (5 vol. %), the samples also contained metal nanoparticles enclosed in a graphite envelope and amorphous carbon particles. The sample was attached to a tungsten filament whose temperature could be varied as a result of ohmic heating. This allowed studying the temperature dependence of the emission current of the nanotubes.

The results of investigations indicate a high sensitivity of the emission characteristics of CNTs to the presence of

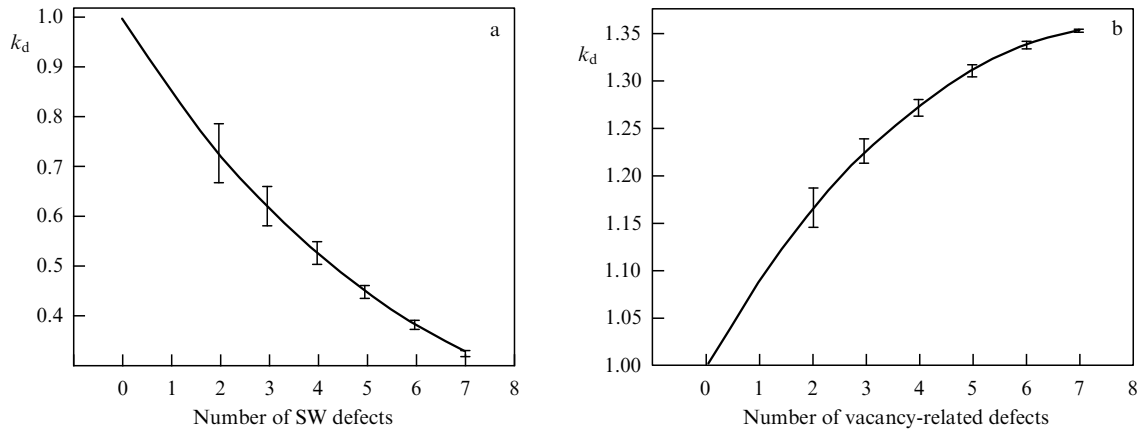

Figure 4. Dependence of the factor k_d on the number of defects of a single-walled nanotube, calculated by the DFT method [54]: (a) Stone–Wells defects, and (b) vacancy defects.

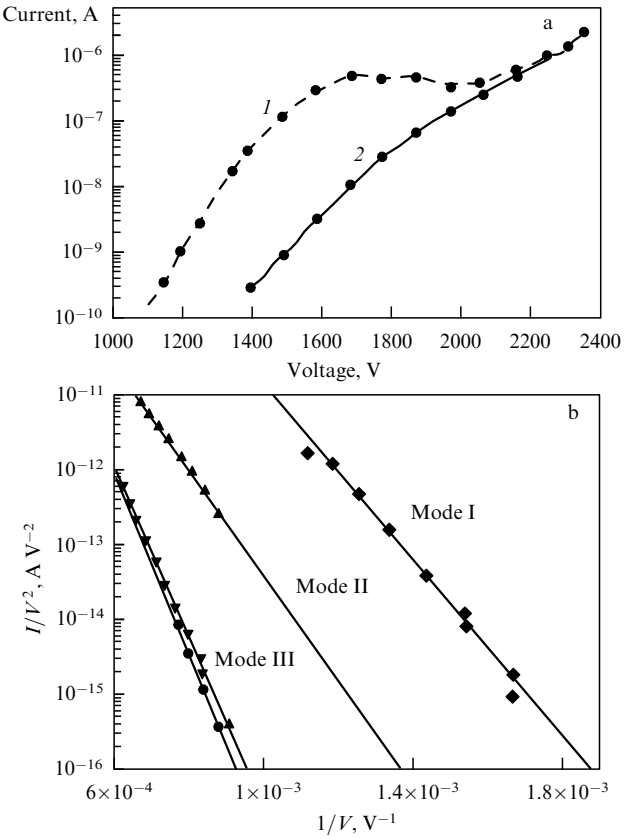

Figure 5. Influence of adsorbates on the emission characteristics of a CNT: (a) current–voltage characteristic of an individual CNT measured in the presence (*1*) and in the absence (*2*) of adsorbates [58], and (b) current–voltage characteristics measured for various operation modes of single-walled CNT-based emitters [57–59].

adsorbates. This is confirmed directly in Fig. 1 presenting the current–voltage emission characteristics of an individual nanotube containing adsorbates and cleansed of them [45]. As can be seen, the removal of adsorbates results in about an order of magnitude decrease in the emission current. This conclusion is in agreement with measurements [57–59] indicating a lowering of the emission current of a CNT-based emitter by as much as two orders of magnitude, as a result of raising the temperature above 900 K. After cooling to room temperature, the initial value of the emission current is restored. The rate of restoring is determined by the content of the residual gas in a vacuum chamber of the emitter. The quadruple mass spectrometry measurements imply traces of H_2 at a residual pressure of 10^{-9} Torr, and traces of H_2O, CO, and CO_2 at a residual pressure of 10^{-10} Torr. Besides these, one should note the presence of adsorbates forming as a result of decomposition of phosphor covering the anode surface under electron irradiation. In this case, the composition of the adsorbates is determined by the composition of phosphor.

The authors of Ref. [59] carried out a direct experiment aimed at establishing the influence of adsorbates on the emission properties of an individual single-walled CNT about 1.7 μm in length. The nanotube was attached to a tungsten filament in the form of a loop. The field emission was observed at an interelectrode spacing of 2 cm. The measurements were performed for both a purified nanotube and for a nanotube whose surface was covered with adsorbates. The adsorbates were introduced through conditioning a purified nanotube for 5 min at a pressure of water vapor of 10^{-7} Torr. This resulted in about a 200-fold increase in the emission current (under an applied voltage of 1400 V). Figure 5a presents the comparison of the current–voltage characteristics of the purified nanotube and the nanotube covered with adsorbates. As can be seen, the nanotube covered with adsorbates demonstrates a saturation of the current–voltage characteristic at a voltage exceeding 1300 V, and a considerable deviation (up to 4 orders of magnitude) from the FN dependence. The current saturation is accompanied by about a 20-fold enhancement of the current fluctuation level. In contrast to the nanotube covered with adsorbates, the emission current for the purified CNT is in good agreement with the FN dependence up to about 2 μA without any indications of saturation. The current–voltage characteristics of the two samples cross at high applied voltages, which indicates the removal of the adsorbates as a result of high-current electron emission.

Figure 5b plots the FN current–voltage characteristics of a single-walled CNT-based emitter observed for the three above-described emission modes. The rectilinear shape of these dependences indicates the field emission mechanism for all the modes. The difference in the slopes of the lines implies a change in the electron work function with a rise in temperature, which also demonstrates the influence of adsorbates on the electronic properties of CNTs.

An analysis of the experimental data indicates that the influence of adsorbates is reduced to the formation of additional electronic states in the electron structure of nanotubes. These states are characterized by a lowered electron work function and therefore promote electron emission at reduced magnitudes of applied voltage.

The occurrence of adsorbates that can escape from the nanotube's surface during the long time the emitter is working is responsible for an unstable operation of the cathode. Thus, notable changes in the emission characteristics of a CNT-based cathode during several hours of operation were observed in Ref. [60]. A paste containing organic and inorganic binders, a photosensitive monomer, and an oligomer (photoinitiator), along with single-walled CNTs, was used as the source of the electron emission. The procedure for preparing the emitter includes the deposition of the paste onto an indium-doped tin oxide (ITO) substrate, drying, point UV irradiation, annealing at a temperature of 450 °C in a nitrogen atmosphere, and the treatment of the surface by means of adhesive tape. The emission was provided by CNT bundles about 10 nm in diameter and between 2 and 5 μm in length. The bundles filled regions about 70 μm in size spaced 450 μm from each other, making up a 22×23 matrix about 0.02 μm^2 in total area. The measurements indicate a dependence of the time evolution of the cathode emission properties on the interelectrode distance. Thus, at the interelectrode spacing of 200 μm the magnitudes of the voltage providing the emission current density of 50, 10, and 150 A cm^{-2} increased during 15 operational hours by 10, 15, and 20%, respectively. As the interelectrode gap increased, the effect of lowering the emission ability of the cathode was weakened. Thus, at the interelectrode spacing of 500 μm the magnitude of the voltage supporting the emission current density at a level of 100 mA cm^{-2} hardly changes. The rise in the voltage that is necessary for supporting some fixed value of the emission current density is one of the manifestations of the emitter degradation resulting from the desorption of adducts.

2.5 Thermal effects

An increase in the temperature of a nanotube as a result of its ohmic heating during emission can change its emission properties. These changes can be reflected in both the transport characteristics of the nanotube (electrical conductivity and thermal conductivity) and its emission capacity. Indeed, a conductor heated to high temperature can emit electrons at very low applied voltages (thermionic emission). This phenomenon is based on the existence in the conductor of high-energy electrons that are able to overcome the potential barrier formed by the ionic lattice. Therefore, one can expect a transition from electron field emission to thermionic emission with a rise in emission current [16]. Such a phenomenon is observed in CNT-based emitters, and the range of parameters where such a transition occurs is quite wide.

The ohmic heating of a nanotube during the emission promotes a thermal inhomogeneity along its length, which can result in the thermal decomposition of the nanotube. This effect limits the maximum reachable emission current and determines the limiting operational characteristics of the relevant cathode. In contrast to conventional electron field emitters, nanotubes are quite elongated objects which hinders the removal of heat from the nanotube to the substrate. This allows the development of thermal instability which results in violation of the thermal balance in nanotubes emitting electrons. The concept of the thermal instability of a CNT-based emitter was framed in Ref. [61], where it was shown that the heat conduction equation for a nanotube emitting electrons has a solution only within a limited range of variability of the emission current. Exceeding some critical magnitude of the emission current causes unlimited heating of the emitter, which is accompanied by its thermal decomposition. The physical reason for developing the thermal instability limiting the emission current of the nanotube is the sharp (exponential) character of the dependence of the emission current on the applied voltage. This exponential dependence is reflected in the dependence of the rate of heat release on the applied voltage. Since the dependence of the rate of heat removal on the applied voltage is not so strong, exceeding some critical value of the emission current leads to the violation of the thermal balance in the nanotube, which is accompanied by its thermal decomposition.

The thermal balance in a nanotube, taking into account ohmic heating, radiation cooling, and heat removal by thermal conductivity, is described by the steady-state heat conduction equation having the following form [62, 63]:

$$\pi r^2 \frac{\mathrm{d}}{\mathrm{d}x}\left(\lambda(T)\frac{\mathrm{d}T}{\mathrm{d}x}\right) - 2\pi r\eta\sigma(T^4 - T_0^4) + \frac{RI^2}{h} = 0\,. \qquad (9)$$

Here, the origin of coordinates ($x = 0$) is found at the point of contact between the nanotube and the substrate; $T = T(x)$ is the temperature profile along the nanotube's axis; $\lambda(T)$ is the longitudinal thermal conductivity coefficient of the nanotube; $R(T)$ is the longitudinal electrical resistance of the nanotube; σ is the Stephan–Boltzmann constant; $\eta < 1$ is the grayness coefficient; r is the external radius of the nanotube, and I is the emission current. The first boundary condition corresponds to the requirement of the equality of the temperature at the point $x = 0$ to the substrate temperature T_0:

$$T(0) = T_0\,. \qquad (10)$$

The second boundary condition is formulated assuming that the nanotube is found in a vacuum, so that the heat flux from the nanotube's tip is zero. This corresponds to the following condition

$$\left.\frac{\mathrm{d}T}{\mathrm{d}x}\right|_{x=h} = 0\,. \qquad (11)$$

The emission current I involved in Eqn (9) as a parameter is interconnected with the applied voltage through the Fowler–Nordheim equation (1).

For the solution of Eqn (9) one needs to have reliable data on the temperature dependences of thermal conductivity $\lambda(T)$ and electrical resistance $R(T)$ along the nanotube's axis. At the present time, such available data are incomplete and contradictory, so that they are characterized by a spread within several orders of magnitude (see review [13] devoted to the transport properties of CNTs). Thus, the values of the thermal conductivity coefficient measured in Refs [64, 65] amount to 3000 and 25 W mK^{-1}, respectively. The electrical resistance of a multiwalled CNT about 100 nm in length varies between 1.5 and 37 kΩ [66]. Investigations indicate that both transport coefficients of CNTs and their temperature dependences are determined by synthesis conditions and can vary within quite a wide range. The reason for such a spread is the occurrence of noncontrollable structural defects in CNTs, as well as adsorbed functional groups having a considerable influence on the electronic structure of the nanotube, phonon spectrum, and other characteristics determining CNT transport properties. Because of the above-mentioned uncertainty, it is hardly possible to obtain the accurate magnitude of the limiting temperature for the emitting nanotube on the basis of Eqn (9).

A convenient approach for representing the temperature dependences of the electrical and thermal conductivities of CNTs is based on the so-called quasiballistic model of transport [13], according to which the charge is carried mainly by electrons, while the heat is transferred mainly by phonons. It being assumed that the ballistic mechanism of charge (heat) transport occurs for a section of a nanotube, whose length l corresponds to the mean free path $l_{\mathrm{e,p}}$ of the electron (phonon) relating to the elastic scattering on defects or admixtures. According to the ballistic mechanism, electrons (phonons) pass this section of the CNT without scattering, and the relevant values of quanta of the ballistic electrical conductivity G_0 and phonon thermal conductivity G_{th} are expressed through the following equations

$$G_0 = \frac{2e^2}{\hbar} = 7.72 \times 10^{-5}\ \Omega^{-1}\,, \qquad (12)$$

$$G_{\mathrm{th}} = \frac{\pi^2 k^2 T}{3\hbar} = 9.46 \times 10^{-13}\ \frac{\mathrm{W}}{\mathrm{K}^2}\ T\,. \qquad (13)$$

Here, G_{th} is the quantum of the phonon thermal conductivity in the limiting case when the characteristic energy of the quantum of phonon vibrations is much less than the temperature T. For obtaining the ballistic thermal conductivity of a CNT, one should multiply G_{th} by the total number of phonon channels N_{p} in the nanotube. The latter is a triple number of atoms in a unit cell, $2N$, where N is expressed through the chirality indices (n, m) of the nanotube in the following way [8, 9]:

$$N = \frac{2(n^2 + m^2 + nm)}{d_{\mathrm{R}}}\,.$$

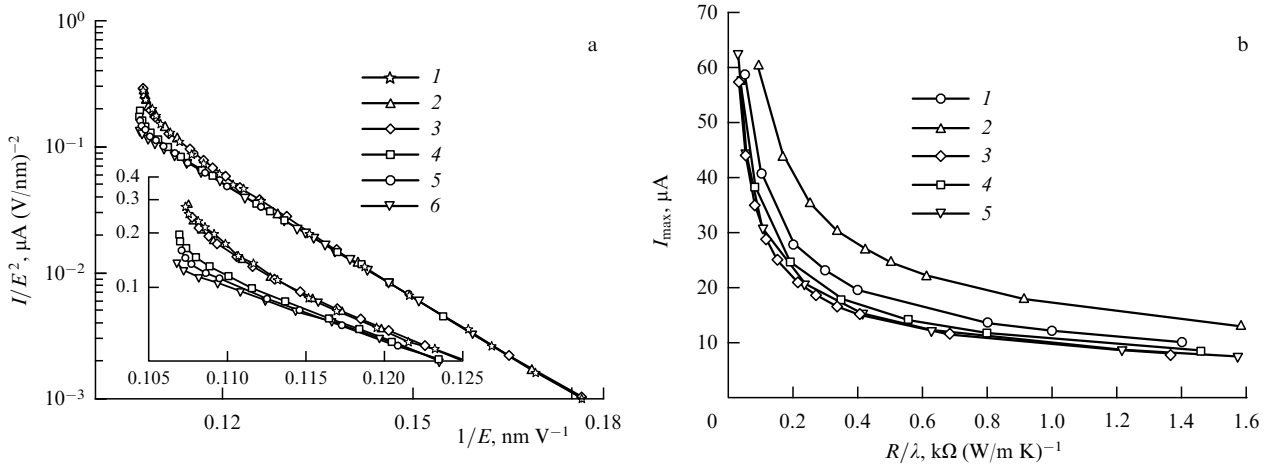

Figure 6. Results of the solution of the heat conduction equation (9) in combination with the Fowler–Nordheim equation (1) [61]: (a) current–voltage characteristics of a carbon nanotube 5 nm in radius and 1.6 μm in length calculated for various model temperature dependences of transport coefficients: *1* — experiment [63]; *2* — $\alpha = 4$; *3* — $\alpha = -1$; *4* — $\alpha = 0$; *5* — $\alpha = 0$, $\lambda = \text{const}$; *6* — $\alpha = 1$. The inset presents an enlarged part of the current–voltage characteristics. (b) Dependences of the emission current I_{max} on the ratio R/λ calculated for various model temperature dependences of transport coefficients: *1* — $\alpha = 0$, $\lambda = \text{const}$; *2* — $\alpha = 4$; *3* — $\alpha = -1$; *4* — $\alpha = 0$, and *5* — $\alpha = 1$.

Here, d_R is the greatest common divisor of $(2n + m)$ and $(2m + n)$. For a single-walled CNT with the *armchair* structure and the chirality indices (n, n), one has $d_R = n$ and $N = 6n$. For example, a single-walled $(10, 10)$ CNT (of diameter 1.4 nm) comprises $N_p = 120$ phonon channels, while a $(200, 200)$ CNT (of diameter 27.5 nm) comprises $N_p = 2400$ phonon channels. Therefore, the ballistic thermal conductivity of $(10, 10)$ and $(200, 200)$ CNTs amounts to $120G_{th}$ and $2400G_{th}$, respectively.

Usually, the nanotube's length h exceeds the characteristic value of the electron (phonon) mean free path $l_{e,p}$ relating to the scattering on structural defects by several times or even by an order of magnitude. In this case corresponding to the quasiballistic regime of charge and heat transport, the above expressions (12), (13) for ballistic transport should be changed by the correcting factor

$$k_{de,p} = \frac{h + l_{e,p}}{l_{e,p}} . \tag{14}$$

Taking account of this correction, the nanotube's resistance R is represented in the form

$$R = \frac{h}{4e^2} \frac{h + l_e}{l_e} , \tag{15}$$

while the CNT thermal conductivity is given by [13]

$$\lambda = \frac{\lambda_0}{k_{dp}} = NG_{th} \frac{l_p}{h + l_p} \frac{h}{\pi r^2} . \tag{16}$$

According to Eqns (15), (16), the transport coefficients of a CNT depend on its length, which can be considered as one of the manifestations of the dimension effect inherent to nanoobjects.

The above-presented consideration shows that the temperature dependences of transport coefficients within the framework of the quasiballistic mechanism of charge and heat transfers are determined by the appropriate dependences of the electron (phonon) mean free path relating to the elastic scattering. The type of structural defects in CNTs determining the character of scattering of electrons and phonons is usually unknown, so that experiment serves as the main source of reliable data on the temperature dependences of transport coefficients [13]. In calculations, the equality $k_{de} = k_{dp}$ is usually accepted, which corresponds to the equality between the electron and phonon mean free paths relating to the scattering on defects and other inhomogeneities. Because of the absence of reliable data on the temperature dependences of transport coefficients, these dependences are usually modeled by a power function:

$$R(T) = R_0 \left(\frac{T}{T_0} \right)^{\alpha} , \tag{17}$$

where R_0 is the resistance at $T = T_0$, and α is the fitting parameter. A similar approach is used for representing the temperature dependence of the thermal conductivity coefficient; however, taking into account the assumption $k_{de} = k_{dp}$, the parameter α has the opposite sign in this case.

Figure 6 presents the results of the solution of the heat conduction equation (9) in combination with the Fowler–Nordheim equation (1), obtained for a nanotube 5 nm in radius and 1.6 μm in length using various assumptions about the temperature dependences of transport coefficients [61]. The calculations indicate that, independently of those assumptions, there exists a maximum reachable emission current whose exceeding results in the development of thermal instability and thermal decomposition of the nanotube. Note that the calculations imply that, even assuming $\eta = 1$, the contribution of radiation losses to the thermal balance of a nanotube does not usually exceed 10%. One can expect that this contribution should increase as the nanotube's length increases. Therefore, taking into account the radiation cooling of a nanotube does not influence qualitatively the above-formulated conclusion on the mechanism of limitation of the emission current, related to thermal instability. The calculated $I-V$ characteristics of a nanotube 5 nm in radius and 1.6 μm in length with a field amplification factor of $\beta = 218.1$ and emitting surface area of $S_{эм} = 12.57$ nm^2 are compared in Fig. 6a with those measured in Ref. [63] for a nanotube of the same geometry.

At low currents, the $I-V$ characteristics in the FN coordinates have a rectilinear shape which corresponds to the classical Fowler–Nordheim dependence. Deviations of the $I-V$ characteristic from this dependence, observed at high emission currents, are caused by the influence of heating the emitter. The character of the deviation is determined by the shape of the temperature dependence of the thermal conductivity or electrical conductivity [fitting parameter α in formula (17)]. A breaking of the $I-V$ characteristic, occurring at some magnitude of the electric field strength, corresponds to the threshold of the thermal instability. The distinctions in behavior of the $I-V$ characteristics calculated within the framework of various models at high currents are explained by the difference in the maximum tip temperature $T_{\max}$ corresponding to the limiting emission current. The higher the nanotube's temperature, the more the deflection of the $I-V$ characteristic from the Fowler–Nordheim dependence, and the sharper the bending of a tail of the curve.

Figure 6b presents the dependences of the limiting emission current $I_{\max}$ on the ratio R/λ, i.e., on the limiting value $T_{\max}$ of the tip temperature, obtained for five models of calculation of $I-V$ characteristics. As is seen, the character of the dependences considered is quite weakly sensitive to the accepted assumption about the temperature dependences of transport coefficients. This indicates the universal nature of the instability under consideration, which manifests itself independently of model assumptions.

Another approach to describing thermal phenomena in CNT-based emitters has been developed by the authors of Ref. [67]. In accordance with their concept, an emitter is destroyed upon reaching the melting point. The critical parameters of emission (current, voltage, and temperature) were calculated using the following approximation of the temperature dependence of the CNT resistivity: $\rho(T) = \rho_0(1 - \alpha T + \beta T^{3/2})$, where the fitting parameters were set equal to $\rho_0 = 3.26 \times 10^{-5}\ \Omega$ m, $\alpha = 8.5 \times 10^{-4}\ \mathrm{K}^{-1}$, $\beta = 9.8 \times 10^{-6}\ \mathrm{K}^{-3/2}$. The thermal conductivity coefficient was taken equal to 100 W m^{-1} K^{-1} and assumed to be temperature independent. The calculated results imply a nonlinear character of dependences of limiting (critical) temperature, electric field strength, and the emission current density on the nanotube's length. Thus, the dependence of the critical temperature on CNT length shows a nonmonotone behavior and takes the minimum value at $h = 19$ μm. A further increase in the nanotube's length is accompanied by a rise in the critical temperature and the critical emission current. This is caused by a lowering of the effectiveness of the heat removal as the nanotube's length increases.

It should be noted that thermal effects can have a considerable influence on the operation of electron field emitters of any nature. However, the thermal instability phenomenon under consideration is apparently inherent to only CNT-based cathodes. Indeed, in contrast to conventional electron field emitters having a conical structure, nanotubes represent 1D conducting systems possessing an elongated cylindrical form. A natural limitation on the rate of heat transport through the cross section of a nanotube exists. As the emission current is enhanced, the heat generation increases, while the rate of heat removal hardly changes and can even decrease in the case of a dropping temperature dependence of the thermal conduction coefficient of the nanotube. This can ultimately result in an unlimited rise in the temperature of the nanotube near its tip and its thermal decomposition.

The influence of thermal effects on the emission properties of CNT-based electron field emitters has been observed in many studies. Thus, the authors of Ref. [68], who studied the emission behavior of an individual multiwalled CNT about 0.5 μm in height and about 10 nm in diameter, observed a catastrophic decomposition of the emitter upon exceeding an emission current of 0.2 mA. However, other researchers [69] claim a lower value of the maximum reachable emission current by about an order of magnitude. Apparently, the thermal stability of CNT-based emitters is rather sensitive to the type and content of defects in nanotubes, which in turn depends on the procedure and conditions of their production.

Thermal decomposition of CNT-based emitters due to ohmic heating during emission has been studied in detail in Ref. [69]. Based on the analysis of experimental data, the authors concluded that the decomposition of CNTs at comparatively low magnitudes of the applied voltage is due to the mechanical failure of the contact between the nanotube and the substrate, while the main reason for decomposition at high values of the applied voltage is the ohmic heating of the emitter. A loose film of multiwalled CNTs grown by the chemical vapor deposition (CVD) method using an Ni or Fe catalyst was utilized as a source of the emission. A metal film 300 nm thick containing Ni or Fe nanoparticles was used as a catalyst. The nanotubes were grown under a hydrogen–methane mixture flow at 570 °C for 15 min. The CNT film produced was placed into the chamber of an SEM at a fixed distance from the anode made from a tungsten wire having a radius of curvature of about 1 μm. Moving the anode above the film surface allowed reaching only a single nanotube whose parameters could be determined by means of the microscope, and which contributed to the emission alone. Measurements evidenced that the current–voltage characteristic of such an emitter at relatively low currents corresponds to the Fowler–Nordheim dependence, reaching saturation as a result of the increase in the current. Further enhancement of the current is accompanied by the thermal decomposition of the emitter. The saturation current amounts to 920 nA for a nanotube 0.66 μm in length and 5 nm in radius, while irreversible thermal decomposition is observed at a current of about 7.5 μA. Treatment of the current–voltage characteristic represented in the Fowler–Nordheim coordinates permitted determining the electric field amplification factor $\beta = 110 \pm 20$ and the area of the emitting surface of 3×10^{-15} m^2, supposing the electron work function of 5.1 eV. Whereas the estimated value of the parameter β is in reasonable agreement with the approximate relation $\beta \sim h/d$, the estimated area of the emitting surface is about 30 times higher than the geometrical cross section of the nanotube.

One more manifestation of the thermal mechanism of nanotube decomposition due to ohmic heating was found in the experiment [69] performed in a two-probe configuration. First, electron field emission occurring in the above-described configuration was observed upon exceeding the voltage across the gap between the nanotube and anode of 112 V. The current–voltage characteristic at low currents is well described by the Fowler–Nordheim equation (1) reaching saturation at a voltage of 160 V, and a current of 50 nA. Then, the open end of the nanotube was put into contact with an anode in order to measure the current–voltage characteristic in the two-probe configuration. The thermal decomposition of the nanotube was evidenced at a voltage of 4 V and a current of 20 μA, so that two parts of the nanotube remained attached to the anode and cathode surfaces. The

field emission from the fragment of the nanotube remained on the cathode surface was observed at a voltage exceeding 43 V, following the Fowler–Nordheim relation until the emitter was destroyed at a voltage of 108 V and a current of 9 μA.

As the emission current rises, the nanotube temperature increases, which changes not only the character but also the mechanism of emission. Along with electron field emission, which is a result of the tunneling of electrons through the barrier formed at the boundary of a conductor, some contribution to the emission is due to thermionic emission, in which case electrons do not oblige to overcome a potential barrier. The relative contribution from the thermionic emission rises as the temperature increases, so that the higher the electric field strength, the higher this contribution. The transition of electron field emission to thermionic emission was studied in detail theoretically by the authors of Ref. [70], who utilized the tight binding approximation to describe the electronic characteristics of a $(12, 0)$ single-walled nanotube. The calculations showed that the field emission mechanism prevails for $T < 1000$ K within the range of the electric field strength $2 < E < 8$ V nm^{-1}, where the current–voltage characteristic is in accordance with the Fowler–Nordheim equation. For $T > 1000$ K, electron field emission prevails as $E < 6$ V nm^{-1}, while at higher fields the contribution of the thermionic emission becomes decisive. Therefore, the relative contribution of thermionic emission has a minimum at $E = 5-6$ V nm^{-1}. Naturally, the position of this minimum depends on the temperature.

Nottingham effect. At quite high magnitudes of the emission current, some contribution to the thermal balance of a nanotube can be made by the cooling of the emitter due to the predominant emission of electrons whose average energy exceeds the relevant equilibrium value that is determined by the emitter's temperature (the Nottingham effect) [71, 72]. This phenomenon takes place at elevated temperatures notably exceeding room temperature, when the probability of tunneling depends essentially on the kinetic energy of an electron. Accounting for the Nottingham effect in the heat conduction equation (9) for a CNT-based emitter results in lowering the emitter's temperature by several percent [62, 72]. However, this effect causes a nonmonotone distribution of the temperature along the nanotube, with a maximum at some distance away from the tip [72]. This promotes the thermal decomposition of the nanotube at the point corresponding to the maximum temperature, which is accompanied by separation of a fragment of about 20% of the nanotube's length. These conclusions obtained on the basis of the solution to the heat conduction equation, taking into account the Nottingham effect, have been confirmed by the results of an experiment [72] performed with an individual nanotube placed into the chamber of a TEM. A nanotube 470 nm in length and 14 nm in diameter attached to a tungsten tip was used as a cathode. The anode was spaced from the nanotube by 800 nm. Separation of a fragment 80 nm in length was observed at an anode voltage of 95 V, and emission current of 35 μA. The failure point turned out to be close to that calculated by solution of the heat conduction equation, taking into account the Nottingham effect.

2.6 Emission from the side wall of a nanotube

It is commonly supposed that the main source of electron field emission is the nanotube's end surface, where the electric field strength has a maximum value. However, this supposition is not confirmed with certainty by the available experimental data. Thus, some authors have concluded on the basis of their experimental data that the side surface of a nanotube surpasses the tip in its contribution to the emission current, while other researchers have made the opposite statement. The emission properties of the side surface of a CNT have been studied in detail by the authors of Ref. [73], who used as a source of emission an individual nanotube about 40 nm in diameter and 10 μm in length synthesized by the CVD method. Irradiation of the nanotube with a Ga ion beam at a current of 500 pA for several seconds resulted in bending the nanotube. At a beam current of several pA, the nanotube was bent into a loop about 300 nm in radius. This loop was inserted into a vacuum camera in order to perform emission measurements which were done at a distance of 150 ± 2 μm between the emitter and the anode. The emission current was limited to a magnitude of 100 nA to avoid degradation of the emitter. This magnitude was reached at the voltage of about 70 V, which corresponds to an average value of the electric field strength in the gap of about 0.5 V μm^{-1}. The measured current–voltage characteristics of the emitter are in good agreement with the Fowler–Nordheim dependence, assuming an electron work function of 5 eV and an electric field amplification factor ranging between 380,000 and 400,000. Such a high magnitude of the field amplification factor is hardly realistic, which can be explained by the phenomenon of lowering the electron work function due to bending the nanotube into a loop and the defect formation induced by the ion irradiation. Since the nanotube bent into the loop has only a side surface, the authors of Ref. [73] reach the conclusion of a high emission ability of such a surface of the nanotube. One can suppose that the reason for such a surprising conclusion is the presence of adsorbates on the nanotube's surface, which, as is known, is accompanied by a notable lowering of the electron work function. In this case, as follows from the Fowler–Nordheim equation (1), the electric field amplification factor estimated on the basis of the current–voltage characteristics of the emitter should be lower than the above-indicated values, while the area of the emitting surface should correspond rather to the whole surface of the nanotube presented to the anode, but not to the end surface.

A similar conclusion has been reached by the authors of Ref. [74], who measured the emission of nanotubes oriented in a different manner relating to the substrate's plane. These nanotubes were applied to a heated filament by means of plasma deposited perpendicular, at an angle of 45°, and parallel to the substrate plane. The measurements showed that in nanotubes oriented parallel to the substrate surface the emission occurs at lower magnitudes of applied voltage than in the other cases. The authors explain this rather surprising result, which contradicts intuitive expectations, by the higher content of defects in the nanotubes oriented parallel to the substrate surface.

The above results [73, 74] contradict the experimental evidence of Ref. [75] presenting a comparison of the contributions from the side and end surfaces of an individual nanotube to the emission current. A multiwalled CNT was affixed to a tungsten tip inserted into a camera of a scanning electron microscope. In some cases, the attached nanotube formed a loop. The measurements showed that the side-wall emission occurs at a magnitude of the applied voltage about 3.8 times higher than that of the end emission.

2.7 Influence of CNT tilting on the electric field amplification

Apart from the possibility of side emission of nanotubes, one can pose the question of the dependence of the emission properties of a nanotube on its orientation with respect to the substrate plane. This question is of great importance because in real conditions the nanotubes making up an emission array can be tilted at various angles to the cathode surface. This is reflected in both the field amplification factor of individual nanotubes and the current–voltage characteristic of the cathode as a whole. This question takes on even greater significance in connection with the action of the electric field on the tilt angle of a nanotube. Taking into account this action results in a dependence of the electric field amplification factor on the local magnitude of the electric field strength in the vicinity of the nanotube's tip. This significantly complicates the form of the current–voltage characteristic of both the individual nanotube and the cathode as a whole.

The dependence of the field amplification factor of an individual CNT on the tilt angle relative to the substrate surface was determined in Ref. [49] on the basis of the solution of the Laplace equation in the vicinity of a nanotube inclined to the cathode surface by some angle. The calculation results allowed reaching a conclusion on the sensitivity of the emission characteristics of a CNT-based cathode to the degree of deflection from the vertical orientation of an individual nanotube. The electric field spatial distribution at the tip of a nanotube inclined to the cathode surface at different angles was calculated by the boundary element method, which is based on Green's integral allowing the determination of the potential at a given point through special integrals taken over the electrode surface [76, 77]. In these integrals, the expression under the integral sign contains the product of an unknown function that is determined by solving integral equations and a fundamental solution to the Laplace equation $\Delta\varphi = 0$ that, in the three-dimensional case, equals unity divided by the distance from a given point to the center of a coordinate system chosen arbitrarily. In this way, the desired potential can be represented as a superposition of potentials produced by virtual charges placed on the surface of a conductor. The arrangement of these charges on the surface is selected so as to provide the spatial potential distribution in the region where this distribution is known.

This approach ensures the adequate behavior of the potential at distances from the emitter surface that exceed the distance between nearby virtual charges. In the region near the emitter surface, the potential distribution is determined by extrapolation from a remote region.

Figure 7 presents the results of numerical calculations of the dependences of the electric field amplification factor on the tilt angle of nanotubes 1 μm in height with various diameters. These dependences are well approximated by the parabolic expression

$$\beta = \beta_0(1 - k\theta^2)\,, \qquad (18)$$

where β_0 is the field amplification factor of a vertically aligned nanotube, determined by its geometry, θ is the angle of CNT inclination, and k is the fitting parameter. The values of the parameters β_0 and k are given in Table 1. As is seen, the magnitude of the fitting parameter k barely depends on the nanotube's diameter.

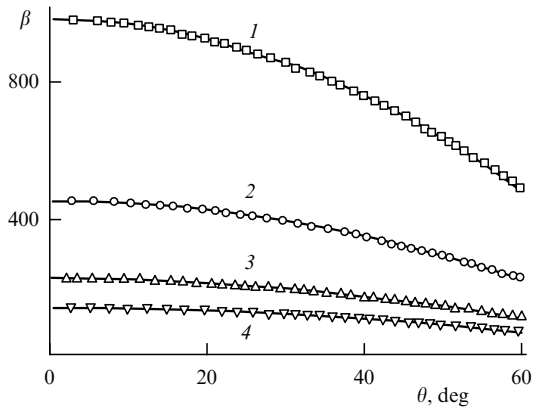

Figure 7. Dependences of the electrical field amplification factor of a nanotube on the tilt angle with respect to the cathode surface, calculated for a nanotube 1 μm in height and with diameters 1.4 nm (*1*); 3 nm (*2*); 6 nm (*3*), and 10 nm (*4*) [49]. Solid lines depict a parabolic approximation of the calculated results in accordance with Eqn (18).

Table 1. The magnitudes of the parameters entering into formula (18), determined for a CNT 1 μm in height and with various diameters [49].

d, nm	1.4	3	6	10
β_0	795	393	209	132
k, 10^{-4}	1.42	1.42	1.42	1.41

2.8 The electron work function of CNTs

The electron work function is one of the most important parameters of a CNT determining its emission properties. It is generally believed that the magnitude of this parameter is close to the relevant value for graphite (about 5 eV). On the one hand, this supposition corresponds to the intuitive notion of the similarity of the electronic structure of CNTs to that of graphite and, on the other hand, it does not contradict numerous experiments on the electron field emission from nanotubes. However, the results of direct measurements are characterized by a considerable spread, which requires caution when using the above-mentioned magnitude. The spread in the electron work function of nanotubes is caused by distinctions in the production conditions of nanotubes, which are followed by differences in both their geometry and the electronic structures. Thus, the hemispherical structure of a nanotube tip can in some cases be either distorted or destroyed completely. This is surely reflected in the electronic properties of the emitter and, in particular, in the relevant value of the work function. Moreover, the nanotube's surface can contain added radicals or molecules, among which should be mentioned H_2O, CO, OH, NO, etc. The occurrence of these adducts promotes the formation of additional electronic states in the electronic structure of CNTs, which can also change the electron work function. It cannot be doubted that even the nanotubes composing the common array are characterized by a considerable spread in the electron work functions. In this connection, the usage of a common value of the electron work function is justified by convenience, and this value can be considered as a result of averaging over some quite wide distribution of data.

Two approaches are invoked for determining the electron work function of CNTs, which often result in rather different data. The first of these (I) is based on processing the measured emission current–voltage characteristics of nanotubes using

Table 2. The electron work function of CNTs measured and estimated by different authors.

Type of nanotube	Diameter, nm	Measurement method	Work function, eV	Ref.
Multiwalled	44	I	7.3 ± 0.7	[78]
Single-walled	1.0 – 1.4	II	4.65 ± 0.1	[79]
Single-walled	1.4	II	4.8	[80]
Multiwalled		II	5.7	[81]
Multiwalled		II	4.3	[82]
Multiwalled	10	II	4.95	[83]
Single-walled	1.4	I	5.1	[84]
Multiwalled	10 – 50	I	0.2 – 2	[85 – 90]

the Fowler–Nordheim expression (1). The application of this approach requires either detailed information about the nanotube structure or additional data about the emitted electron energy distribution. The second approach to evaluating the electron work function of CNTs (II) is based on the determination of the energy spectrum of photoelectrons emitted upon optical irradiation of the material surface. The lower edge of the spectrum corresponds to the electron work function.

Table 2 contains the quantities of the electron work function of CNTs measured and estimated by different authors. As can be seen, in most cases the electron work function for nanotubes is close to the relevant magnitude for graphite, which ranges between 4.4 and 5 eV. A notable distinction between the magnitudes of the work function for single-walled and multiwalled nanotubes was not observed. The values of the work function ($\varphi = 0.2 - 2$ eV) estimated by the authors of Refs [85–90] are markedly different from the total mass of data. However, these estimates are rather indirect, and their results are very sensitive to the values of the radius of curvature of the emitter used in the calculation, which are determined in this context on the basis of visual analysis of microphotographs and hardly can be believed as plausible. One can suppose that in this case the electron emission originates from an open end of a nanotube, so that the characteristic size of the emitting surface is several times smaller than the diameter of the nanotube, which is used in estimating the electron work function.

The statistical treatment of the electron work function data given in Table 2 results in the average value of $\varphi = 5.26 \pm 0.85$ eV. As follows from the analysis of studies focused on determining the electron work function of CNTs, many questions related to this problem remain unsolved. Specifically, it is unclear how this quantity depends on both the diameter and chirality of a single-walled nanotube. It is not established what determines the electron work function of a multiwalled nanotube consisting of single-walled nanotubes with different magnitudes of the work function. There are no data in hand about the dependences of the electron work function on the position of the emitting area on the nanotube surface, on the bending angle of the nanotube, and on structural defects on the surface of single-walled and multiwalled nanotubes. One can hope that further studies focused on answering these and other similar questions, coupled with the development of methods for the synthesis of nanotubes with specified structural parameters, should provide a possibility for producing CNT-based electron field emitters having well-defined emission characteristics.

Some notion of the degree of sensitivity of the electron work function to structural peculiarities of CNTs can be obtained analyzing the results of calculations performed by the authors of Ref. [91] with the usage of the density functional theory (DFT). They calculated the work function for nanotubes having the chirality indices $(3, 3)$ and $(5, 0)$ and closed caps, as well as for nanotubes with added H radicals, as a function of the distance between individual nanotubes. The calculated results imply that the magnitude of this parameter significantly depends on both the nanotube's length and occurrence and the arrangement of added radicals. In particular, the electron work function (5.7 eV) of the $(3, 3)$ nanotubes bound into bundles exceeds approximately by 15% the relevant value for an individual CNT, as well as for CNTs spaced at a distance of 1.5–3.0 nm from each other. Another situation takes place in the case of nanotubes of the same chirality with added hydrogen radicals. The work function of such objects bound into bundles (about 3 eV) is roughly 25% lower than that for individual nanotubes spaced at 1.5–3.0 nm. Bounding the nanotubes with chirality $(5, 0)$ does not change so notably the electron work function, and therefore it does not show the dependence on the intertube distance in this case. The dependence of the electron work function on the intertube distance in a bundle can be utilized as a basis for the development of CNT arrays with a controllable value of the electron work function.

3. Emission characteristics of CNT arrays

A CNT array usually contains a huge number of individual nanotubes. These emitters differ from each other in their geometry, degree of alignment, electronic properties, etc. Because of the sharp dependence of the emission current of an individual nanotube on the electric field strength in the vicinity of its tip, the main contribution to the emission is conventionally due to a relatively few number of nanotubes having the maximum magnitude of the field amplification factor β; these are usually the highest nanotubes protruding from the array. The relative contribution of the rest of the nanotubes increases as the applied voltage grows. Therefore, the emission properties of a cathode combine the current–voltage characteristics of individual nanotubes but can differ essentially from the Fowler–Nordheim dependence (1). In addition, the electric field in the vicinity of an individual nanotube of the array can be notably distorted due to the screening action of surrounding neighbors. As a result of this action, the electric field amplification factor β of a nanotube involved in the array should depend not only on its aspect ratio and interelectrode spacing but also on the geometry of the array and the nanotube's density in it. The screening effect manifests itself in a nonmonotone dependence of the emission current density on the surface density of nanotubes in the array. The maximum emission current density is reached at the average intertube distance, which is on the order of the height of individual nanotubes making up the array. The emission characteristics of CNT-based cathodes will be considered below, taking into account the above-mentioned effects of statistical spread, screening, and some other phenomena of both physical and technical origins.

3.1 Screening effects

One can single out several types of arrangements of nanotubes in an array. Three of them are shown in Fig. 8 [30]. The character of the emission from a rarefied homogeneous array of vertically aligned nanotubes (upper picture) is similar to that occurring in an individual CNT. This means that the distribution of the electric potential in the vicinity of

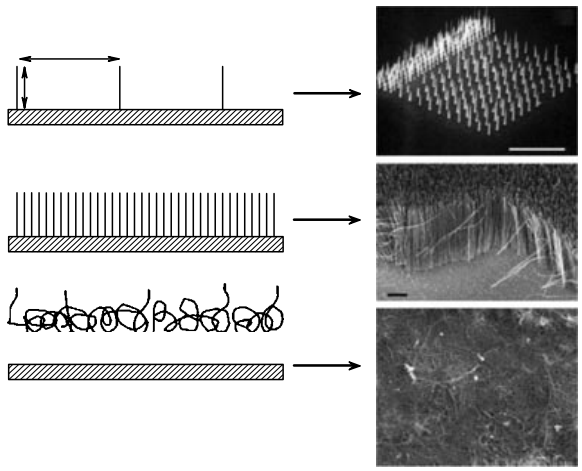

Figure 8. Various types of arrangements of CNTs in field emission cathodes [30]: top — low-density array whose emission behavior corresponds to that of an individual nanotube; middle — a dense array of vertically aligned nanotubes, for which the emission current density depends on the array's density in a nonmonotone manner; bottom — a film of disordered highly entangled nanotubes, for which the emission current density is determined by the number and structure of the mostly protruding nanotubes.

the tip of each individual nanotube in the array does not experience the disturbing action of neighboring nanotubes, so that the total emission current is the result of the summation of the contributions from all the individual nanotubes. In the case of a homogeneous array of closely packed vertically aligned nanotubes (middle picture), the electric potential formed in the vicinity of the tip of each nanotube is screened by neighboring nanotubes, so that the electric field strength depends notably on the density of nanotubes in the array. This leads to a nonmonotone dependence of the emission current density on the density of nanotubes in the array. This dependence can be evaluated on the basis of the solution of the 3D Laplace equation for arrays of various densities. The third type of the arrangement of CNTs in the array displayed in Fig. 8 refers to a disordered film of entangled nanotubes of various geometries. Such a type of emitter is rather complicated for analysis. It should be noted that the emission properties of such a film are determined mainly by the nanotubes protruding from the array. The number of such emitters is relatively small and the character of their emission is rather unstable and nonreproducible, so that this kind of emitters is characterized by a relatively low level of emission current density, which is determined by the number and the structure of the most notably protruding nanotubes. Therefore, one should believe that the optimum arrangement of nanotubes corresponds to an array of vertically aligned emitters with moderate number density, for which the screening effect has relatively weak influence.

The dependence of the emission current density on the intertube distance in the array was first determined by the authors of Ref. [92], who calculated the electric potential for an array of vertically aligned nanotubes as a function of the intertube distance using the 3D Laplace equation. In doing so, the authors established the dependence of the emission current density on the average intertube distance and found the optimal value of this parameter, which turned out to be close to double the height of the nanotube. This result differs somewhat from the conclusion obtained in Ref. [46] on the basis of solution of the Laplace equation for a 2D array of similar vertically aligned nanotubes 1 nm in diameter and 1 μm in height having a flat cap. The results of these calculations presented in Fig. 9 imply that the optimum value of the average intertube distance providing the maximum emission current density is about half the nanotube's height.

Subsequent studies [93–95] have shown that the quantitative difference in the results of the cited Refs [46, 92] is due to the sensitivity of the form of dependence of the emission current density on the intertube distance in the array to the magnitude of the applied voltage. This relates to the nonlinear character of the Fowler–Nordheim equation (1) interconnecting the emission current and the voltage across the gap. Therefore, the form of the mentioned dependence is determined by the applied voltage. The value of this parameter is not usually indicated in publications, which can result in misunderstandings.

A more complicated character of screening manifests itself in a quite spread case when the emitter consists of bundles, each involving several dozen nanotubes, but not of isolated CNTs. The computer simulation of such a case meets with considerable calculation difficulties; therefore, the main

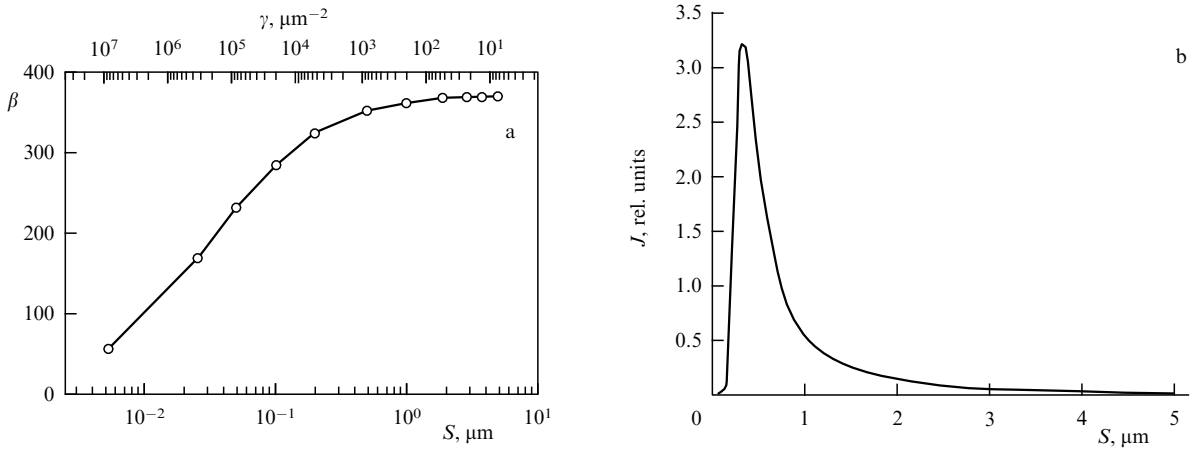

Figure 9. Results of the solution of the Laplace equation for a 2D array of similar vertically aligned nanotubes 1 nm in diameter and 1 μm in height having a flat cap [46]: (a) dependence of the electric field amplification factor of a nanotube involved in the array on the average intertube distance S and the surface density γ of nanotubes; (b) dependence of the emission current density of the CNT array on S, calculated taking into account the screening effect.

source of information in this situation is experiment. The phenomenon of the electric field amplification for a cathode consisting of CNT bundles of various diameters was studied in detail in Ref. [96] taking into account the screening effect. Three hundred twenty individual vertically aligned CNT bundles about 100 μm in height and 120, 60, 30, and 15 μm in diameter were placed in a regular manner 200 μm apart on a substrate 3600×3600 μm in size. The nanotubes were grown on a silicon substrate utilizing the CVD method under an $H_2 + C_2H_2$ flow at a temperature of 700 °C with the usage of an iron-based catalyst. The diameter of a bundle was determined by the size of the catalyst particle. The individual nanotubes forming the bundles ranged from 10 to 15 nm in diameter consisted of 5–7 graphite layers, and were spaced, on average, about 50 nm apart. The emission properties of the cathode were studied with the usage of an anode of a cylindrical tungsten probe 150 μm in diameter having a flat cap. Therefore, the surface area of the anode was much larger than the cross section of any bundle, but the anode size still remained shorter than the interbundle spacing. The emission current was measured at an interelectrode distance of 100 μm. The results of measurements indicate a strong dependence of the current–voltage characteristics of the emitter on the bundle diameter. Table 3 presents the values of the electric field strengths E_{t0} and E_{th} averaged over the gap, providing an emission current density at the levels of 10 μA cm^{-2} and 10 mA cm^{-2}, respectively. The values of the electric field amplification factor β obtained as a result of treating the current–voltage characteristics are also listed.

Table 3. The values of the electric field strengths E_{t0} and E_{th} averaged over the gap, providing the emission current density at the levels of 10 μA cm^{-2} and 10 mA cm^{-2}, respectively, and the values of the electric field amplification factor β obtained as a result of treating the current–voltage characteristics [96].

Bundle diameter, μm	E_{t0}, V μm^{-1}	E_{th}, V μm^{-1}	β
400	6.7	11.6	602
120	5.6	8.7	639
60	4.1	7.9	1013
30	2.9	6.2	1726
15	1.6	2.5	2425

As is seen from the data given in the table, the less the bundle diameter, the lower the magnitude of the applied voltage promoting emission. It is of interest to note that the estimated values of the electric field amplification factor exceed by about two orders of magnitude the aspect ratio of the bundle. However, these values are several times lower than the relevant value of $\beta \approx 10{,}000$ for an individual nanotube. Therefore, the usage of nanotube bundles as emitters allows one to overcome one of the most serious problems relating to the electrostatic screening of nanotubes.

One more effective approach to the enhancement of the electric field amplification factor of individual CNTs has been demonstrated by the authors of Ref. [97], who grew single-walled or thin multiwalled CNTs on the tips of large-diameter multiwalled CNTs, which resulted in a notable improvement in the emission characteristics of a CNT-based cathode. As a substrate, a porous silicon wafer 5 cm in diameter and 300 μm thick was utilized. Its resistivity ranged between 0.008 and 0.02 Ω cm, and the diameter of the pores amounted to 15–20 nm. The substrate was applied with a thin (10 nm) layer of Fe used as a catalyst. To provide a contact of catalyst particles with nanopores, the sample was annealed at a temperature of 300 °C for 12 h. Multiwalled vertically aligned nanotubes 55 μm in height and 15–20 nm in diameter were grown at a temperature of 700 °C for 40 min under the flow of acetylene. Fe particles were deposited onto the tips of these CNTs by means of a shadow mask for the purpose of growing nanotubes of smaller diameter. Samples of the substrates prepared in such a manner were placed into a CVD chamber where single-walled and thin multiwalled nanotubes 10–15 μm in height and 2–10 nm in diameter were grown under the flows of methane (1000 cm^3 min^{-1}) and ethylene (5 cm^3 min^{-1}) at a temperature of 900 °C for 5 min.

The emission characteristics of the cathodes prepared were measured in a diode configuration at an interelectrode spacing of 900 μm and a residual gas pressure of about 10^{-6} Torr. The current–voltage characteristics of cathodes consisting of multiwalled CNTs and multiwalled CNTs with CNTs of lower diameter at the ends proved to be in good agreement with the Fowler–Nordheim equation. However, the emission current for two-step nanotubes exceeds that for initial multiwalled nanotubes by ten times at the same magnitude of applied voltage. Treatment of the emission characteristics in the Fowler–Nordheim coordinates has indicated that the usage of two-step emitters results in the enhancement of the field amplification factor from 8400 to 26,200. Therefore, changing the nanotube's geometry offers a possibility of improving the operational characteristics of an emitter.

3.2 Statistical spread of CNT parameters

As follows from the above analysis, the emission characteristics of CNTs are very sensitive to their individual parameters, like the height, diameter, electron work function and so on. The natural spread in the values of these parameters caused by both the synthesis conditions and changes in the course of the operation promotes notable deviations of the current–voltage characteristics of a CNT array from the Fowler–Nordheim dependence (1) inherent to an individual emitter. A simple approach illustrating the influence of the statistical spread of CNT parameters in the current–voltage characteristics of a cathode has been developed in Ref. [98]. There it was supposed that the statistical spread of the electric field amplification factor β of individual nanotubes is described by a normal distribution. The current–voltage characteristic of an individual nanotube obeys the Fowler–Nordheim equation

$$J(E_0, \beta) = C_1 \beta^2 E_0^2 \exp\left(-\frac{C_2}{\beta E_0}\right),$$

where E_0 is the magnitude of the electric field strength averaged over the gap. Due to the statistical spread of the parameter β, the magnitude of the electric field strength in the vicinity of the nanotube's tip also has a spread which promotes a distinction of the current–voltage characteristic of the cathode from the Fowler–Nordheim function (1). This distinction can be described through a simple model based on the normal distribution of the parameter β:

$$P(\beta) = \frac{1}{\Delta\beta\sqrt{\pi}} \exp\left[-\frac{(\beta - \beta_0)^2}{\Delta\beta^2}\right]. \qquad (19)$$

Here, $P(\beta)$ is the probability density of a specific value of β; β_0 is the average magnitude of this parameter, and $\Delta\beta$ is the

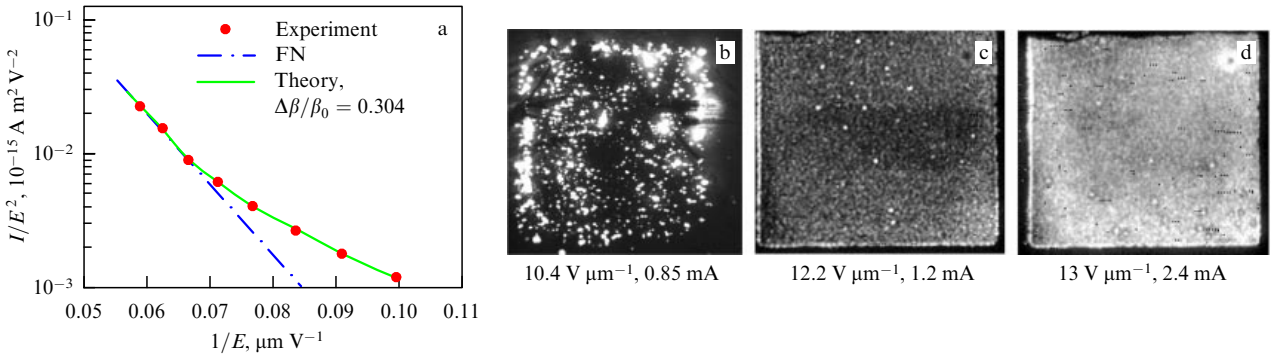

Figure 10. Illustration of the influence of the statistical spread of CNT parameters on the operating characteristics of a field emission cathode: (a) comparison of the Fowler–Nordheim characteristic (dashed-dotted line) with the calculated results obtained on the basis of generalized equation (23) (solid line), and with the measured data [99] (dots); (b)–(d) the images of the distribution of the luminescence intensity over the phosphor surface, obtained at various values of the electric field strength and the emission current [99].

variance. The emission current density is represented as a result of statistically averaging the current–voltage characteristic (1), taking into account the probability distribution (19):

$$J = \int_0^\infty P(\beta)\, J(\beta)\, \mathrm{d}\beta$$

$$= \int_0^\infty \frac{C_1 E_0^2 \beta^2}{\Delta\beta\sqrt{\pi}} \exp\left[-\frac{C_2}{\beta E_0} - \frac{(\beta-\beta_0)^2}{\Delta\beta^2}\right] \mathrm{d}\beta\,. \qquad (20)$$

This integral is easily calculated analytically under the conditions

$$\Delta\beta \ll \beta_0\,, \qquad \frac{C_2}{E_0\beta_0} \gg 1\,. \qquad (21)$$

First, in this case the low integration limit can be extended down to $-\infty$. Second, the smooth pre-exponent dependence under the integral sign can be neglected, in comparison to the sharply changing exponent. Third, the first item under the exponent sign can be represented by the following expansion:

$$\frac{C_2}{\beta E_0} \approx \frac{C_2}{\beta_0 E_0}\left(1 - \frac{\beta-\beta_0}{\beta_0}\right). \qquad (22)$$

The calculation of integral (20) taking account of the above simplifications results in the following relation

$$J = C_1 E_0^2 \beta_0^2 \exp\left(-\frac{C_2}{\beta_0 E_0} + \frac{C_2^2 \Delta\beta^2}{4\beta_0^4 E_0^2}\right). \qquad (23)$$

This can be considered as a generalized Fowler–Nordheim equation. This expression contains two factors, one of which corresponds to the classical Fowler–Nordheim equation (1) and prevails at relatively high fields, such that

$$E_0 \gg \frac{C_2}{4\beta_0}\frac{\Delta\beta^2}{\beta_0^2}\,, \qquad (24)$$

while the contribution of the second factor becomes notable at low fields obeying the opposite condition. Representation of Eqn (23) in standard Fowler–Nordheim form results in

$$\ln\frac{J}{E_0^2} = \ln\left(C_1\beta_0^2\right) - \frac{C_2}{\beta_0 E_0} + \frac{C_2^2(\Delta\beta)^2}{4\beta_0^4 E_0^2}\,. \qquad (25)$$

As is seen, the right-hand side of this equation contains, in addition to the linear dependence, a quadratic dependence on the inverse electric field strength.

The above dependence (23) was used for treating the current–voltage characteristics of CNT-based field emission cathodes with the aim of determining the degree of homogeneity of parameters of individual emitters. A typical current–voltage characteristic of this kind is presented in Fig. 10a in Fowler–Nordheim coordinates [99]. As is seen, in the region of comparatively high fields this dependence has practically a rectilinear form, which is in agreement with the Fowler–Nordheim equation (1). In a low-field region, this characteristic shows a notable deviation from (1), which is caused by the statistical spread of the CNT parameters. The measured data agree with Eqn (25) at $\Delta\beta/\beta_0 = 0.304$.

The above analysis indicates that, due to the natural statistical inhomogeneity of a CNT array, a relative number of nanotubes contributing to the emission current depends on the electric field strength. In low fields only a few of the most protruding nanotubes having a quite high magnitude of the electric field amplification factor can emit electrons. As the field strengthens, the number of such nanotubes increases, so those nanotubes with a moderate value of β are able to contribute to the emission. In very strong fields, practically all the nanotubes are involved in the emission. These considerations have been confirmed directly in experiment [99], where single-walled nanotubes synthesized in an electric arc chamber 7 l in volume using an Ni/Cr catalyst [100] were used as a source of the electron emission. In the synthesis of CNTs, a cylindrical graphite rod 6 mm in diameter with a sharpened end was utilized as a cathode. As a consumable anode, a 'sandwich' structure was used consisting of two graphite rods having a rectangular cross section (7 × 3.5 mm) with a thin Ni/Cr (mass ratio 80/20) catalyst foil 0.2 mm thick. The mass of the foil amounted to about 10% of the mass of the anode material. Such an anode structure provides a homogeneous supply of the catalyst to the plasma region. The dc discharge was burnt at an He pressure of 700 Torr, current of 60 A, voltage of 29–30 V, and interelectrode distance of 4 mm. The setup was equipped with devices for the automatic stabilization of voltage and interelectrode gap. The rate of thermal sputtering of the anode material was about 1 g h^{-1}.

As a result of the long discharge burning the chamber walls were covered with a material containing single-walled CNTs. This material had a layered cloth-like structure with a

Table 4. Relative dispersion of the magnitudes of the electric field amplification factor, $\Delta\beta/\beta$, determined through treating the experimental data for CNT-based electron field emission cathodes [98].

Type of CNT	Diameter, nm	Emitter density, cm^{-2}	Interelectrode gap, mm	$\Delta\beta/\beta$	Voltage range, kV	Current range, μA	Ref.
Single-walled	5	10^5	5 – 20	0.24	5 – 15	$10^{-4} - 10^2$	[101]
Single-walled	1 – 2	10^5	0.006	0.16	0.01 – 0.02	$10^{-4} - 10^2$	[102]
		10^5	0.002	0.105	0.02 – 0.07	0.1 – 5	[103]
Single-walled	1.2		0.25	0.103	0.2 – 0.4	$10^{-6} - 1$	[104]
Multiwalled	25		0.25	0.13	0.4 – 0.7	$10^{-6} - 0{,}1$	[104]
Multiwalled	20		1	0.18	0.02 – 0.04	0,1 – 5	[105]
Single-walled	1 – 1.5		0.5	0.304	0.1 – 9	$10^{-2} - 10^2$	[99]

porosity of about 90%. It could be easily separated from the wall and retained its stability against simple mechanical actions. The growth rate of such a layer was about 0.1 mm h^{-1}. The material produced was studied by Raman spectroscopy, transmission electron microscopy, and thermogravimetry. In addition, the sample was subject to an acid treatment. Measurements showed that the synthesized samples contained single-walled CNTs up to 5 μm in length and ranging between 1.2 and 1.5 nm in diameter, with the average value of about 1.24 nm. The nanotubes were bound into bundles about 10 nm in diameter consisting of about 100 individual CNTs. The material was highly contaminated with carbon nanoparticles and metal catalyst particles, which can be mostly removed through thermal treatment in oxygen or air.

Samples of the soot containing CNTs were used for fabrication of a field emission cathode. For this purpose, the soot was annealed in air at 600 °C, followed by powdering in an agate mortar. The finely dispersed powder produced in such a manner was used to obtain a suspension on the basis of CCl_4. This suspension was applied to a silicon or copper substrate 1×1 cm in area and was dried at room temperature. This resulted in the formation of single-walled CNT films having an adhesion sufficient for emission measurements.

The emission characteristics of cathodes fabricated by the above method were measured in Ref. [99] by means of a wide-aperture diode device. As an anode was used a glass plate covered with a phosphor layer and a conducting layer on the basis of indium–tin oxide (ITO). The measurements were performed at an interelectrode spacing of 500 μm and a residual gas pressure lower than 10^{-6} Torr. The magnitude of the pulsed voltage applied to the gap was up to 9 kV at a pulse duration of 100 μs and a pulse repetition rate of 50 Hz. The distribution of the emission current density over the anode surface promoted the relevant luminescence of the phosphor, which was photographed and recorded. One should note the high sensitivity of the emission character to the thickness of the soot layer at the substrate. Thus, emission is not observable at a thickness exceeding 0.3 mm.

A typical current–voltage characteristic of the cathode is shown in Fig. 10a in the Fouler–Nordheim coordinates. The deviation of this dependence from the Fowler–Nordheim function observed in low fields ($E \leqslant 10$ V μm^{-1}) was considered above and relates to the statistical spread of the parameters of individual CNTs. Due to this phenomenon, only a minor fraction of the nanotubes protruding from the array contribute to the emission at low fields. The direct confirmation of this effect follows from a comparison of distributions of the intensity of luminescence over the anode surface, obtained at various magnitudes of the applied voltage and presented in Figs 10b–d. As is seen, an increase in the electric field strength results not only in enhancement of the luminescence brightness, but also in an increase in the area of the shining surface.

The above-derived interrelation between the shape of the current–voltage characteristic of a CNT-based cathode and a relative dispersion of the parameters of individual emitters permits determining the degree of inhomogeneity of a CNT array by processing the current–voltage characteristics. Table 4 presents the results of such a processing performed for several current–voltage characteristics of CNT-based field emission cathodes, measured by various authors. As can be seen, the magnitude of the relative spread of the parameter $\Delta\beta$, determined by processing various measurement data, varies within the region $\Delta\beta/\beta = 0.1 - 0.3$. Taking into account the sharp exponential dependence of the emission current on this parameter, one can conclude that the cathodes under consideration are characterized by a rather high degree of surface inhomogeneity. Notice that the above-stated interrelation between the degree of inhomogeneity of a cathode and the shape of its current–voltage characteristic can be used for the analysis of the quality of a CNT array designed for a purpose not necessary related to field emission.

The statistical spread of the emission properties of individual CNTs can be caused not only by a difference in their geometric parameters, but also by differences in the angles of inclination of nanotubes with respect to the substrate surface. In this case, as was shown above [49] [see Eqn (18) and Fig. 7], the electric field amplification factor of an individual CNT depends on the angle of inclination. This can promote a deviation of the current–voltage characteristic of the cathode from the Fowler–Nordheim dependence, so that the degree of deviation is determined by both the spread of the angles of CNT inclination and the average value of this parameter.

The current–voltage characteristics of a CNT-based cathode, taking account of the statistical spread in the angles of inclination, were calculated in Ref. [49]. In so doing, the above dependences of the electric field amplification factor on the angle of inclination of the nanotube were used. The tilt angle distribution of CNTs was supposed to obey the Poisson function

$$\mathrm{d}P(\theta) = A\,\frac{\mathrm{d}\theta}{\bar{\theta}}\exp\left(-\frac{\theta}{\bar{\theta}}\right), \tag{26}$$

where $\bar{\theta}$ is the average value of the angle of inclination, and the factor

$$A = \left[\int_{0^\circ}^{90^\circ}\frac{\mathrm{d}\theta}{\bar{\theta}}\exp\left(-\frac{\theta}{\bar{\theta}}\right)\right]^{-1} = \left[1 - \exp\left(-\frac{90^\circ}{\bar{\theta}}\right)\right]^{-1} \tag{27}$$

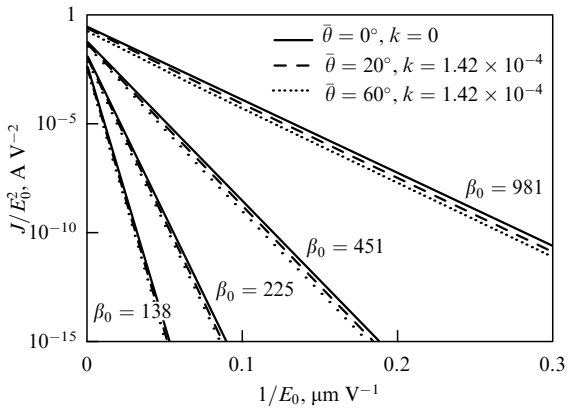

Figure 11. Current–voltage characteristics of a CNT-based cathode calculated taking into account the nanotube's inclination according to formula (11) [49]. The case disregarding the inclination effect corresponds to $\bar{\theta} = 0$.

is determined by the normalization relation

$$\int_{0°}^{90°} \mathrm{d}P(\theta) = \int_{0°}^{90°} \frac{A}{\bar{\theta}} \exp\left(-\frac{\theta}{\bar{\theta}}\right) \mathrm{d}\theta = 1\,. \tag{28}$$

In the limiting case of $\bar{\theta} \ll 1$, the value of A is close to unity. Thus, $A(\bar{\theta} = 20°) = 1.011$. The emission current density for a CNT array with randomly distributed angles of inclination is expressed through the obvious integral

$$\begin{aligned} J &= \int_{0°}^{90°} I_{\mathrm{FN}}(E)\, N\, \mathrm{d}P(\theta) \\ &= \int_{0°}^{90°} I_{\mathrm{FN}}(E_0\beta_0(1 - k\theta^2))\, \frac{SN}{\bar{\theta}} \exp\left(-\frac{\theta}{\bar{\theta}}\right) \mathrm{d}\theta\,. \end{aligned} \tag{29}$$

Here, $I_{\mathrm{FN}}(E)$ is the emission current of an individual nanotube, determined by the Fowler–Nordheim equation (1) and taking into account the dependence of the electric field amplification factor on the angle of inclination θ (18) and the random distribution (26) of CNTs over the angles of inclination, and N is the number of nanotubes per unit area of the emitter.

Figure 11 presents the current–voltage characteristics of a cathode calculated on the basis of Eqn (29), taking account of the spread of CNTs in the angle of inclination for various average values of this parameter. As can be seen, even for a large magnitude of $\bar{\theta} = 60°$ the deviation of the calculated dependence from the Fowler–Nordheim function is rather small compared to that related to the statistical spread in the geometric parameters of CNTs (cf. Fig. 10a).

4. CNT-based cathodes and their applications

4.1 Maximum emission current density

The maximum reachable magnitude of the emission current density for a CNT-based cathode can be roughly estimated from the following considerations. The maximum density of nanotubes at a substrate is restricted by the screening effects, whereby the optimum intertube distance in an array is about the nanotube's height. Thus, for a CNT array 1 μm in height the optimum density of emitters is about 10^8 cm^{-2}. The maximum reachable value of the emission current for an individual nanotube is limited by thermal effects and amounts to about 1 μA. Therefore, the maximum reachable value of the emission current density for a CNT-based cathode is estimated as 100 A cm^{-2}. Such high values of the emission current density are hardly reachable in reality for large-sized cathodes in steady-state conditions. The main reasons for such a contradiction include, first, the violation of the homogeneous character of distribution of nanotubes over the cathode surface, as well as the rather low degree of their vertical orientation. Due to these factors, a notable contribution to the total emission current is made by only a few nanotubes protruding from the array and possessing the maximum value of the electric field amplification factor. Moreover, the thermal removal is hindered in a dense CNT array; therefore, the thermal limitations of emission current occur at considerably lower currents than in the case of individual nanotubes. One can conclude that the maximum magnitude of the emission current density can be reached only as a result of the thorough preparation of the cathode, ensuring a high degree of surface homogeneity and vertical alignment of the nanotubes. For this reason, the maximum value of the emission current density reported in many publications is much lower than the result of the above-performed estimation. Below, systems for which the emission current density exceeds 1 A cm^{-2} will be analyzed.

Emission with a current density at the level of several amperes per centimeter has been reported in many publications (see, e.g., Refs [106–109]). Thus, Ref. [106] presents the procedure for fabricating and testing a cathode with an emission current density up to 2.8 A cm^{-2}. Vertically aligned CNT bundles were grown by using the CVD method combined with a photolithography application of catalyst particles. Fe particles 1 nm in size and Al particles 10 nm in size were applied to regions of a stainless steel substrate 50 μm in diameter at room temperature using photolithography and electron beam evaporation. The samples produced were annealed for 1 h, followed by the CVD procedure at a temperature of 650 °C and a pressure of 4.5 Torr. A mixture of C_2H_2 and He in the ratio of 1 : 4 flowing at the rate of 100 cm^3 s^{-1} (sccm) was used as an operating gas. This procedure resulted in the growth of 5 bundles consisting of multiwalled CNTs about 4 nm in internal diameter and about 9 nm in outer diameter. Bundles about 50 μm in diameter and about 70 μm in height were spaced 3 mm from each other. The density of CNTs in the bundles was about 10^{10} cm^{-2}. The emission properties of a cathode fabricated in such a manner were studied at a vacuum level of 10^{-7} Pa.

Figure 12 presents the emission current–voltage characteristic of the bundles. The magnified part of this dependence corresponding to the current density region $J < 50$ mA cm^{-2} is shown in the inset to the figure. The emission current density was determined by dividing the measured current by the total cross section of 5 bundles (1.96×10^{-5} cm^2). The threshold value of the electric field strength, E_{th}, providing the current density of $J = 10$ mA cm^{-2} is equal to 2.0 V μm^{-1}. At $E = 2.9$ V μm^{-1}, the current density equals $J = 2.8$ A cm^{-2}. The current–voltage characteristic is in good agreement with the Fowler–Nordheim dependence, which confirms the field origin of the emission observed. Treatment of this dependence, assuming the electron work function for CNTs to be 5 eV, results in an estimated magnitude of the electric field amplification factor $\beta \approx 2500$. The stability of the emission properties of the emitter was studied in high-vacuum conditions at an electric field strength of 2.4 V μm^{-1}. The measurements showed that the emission current per bundle

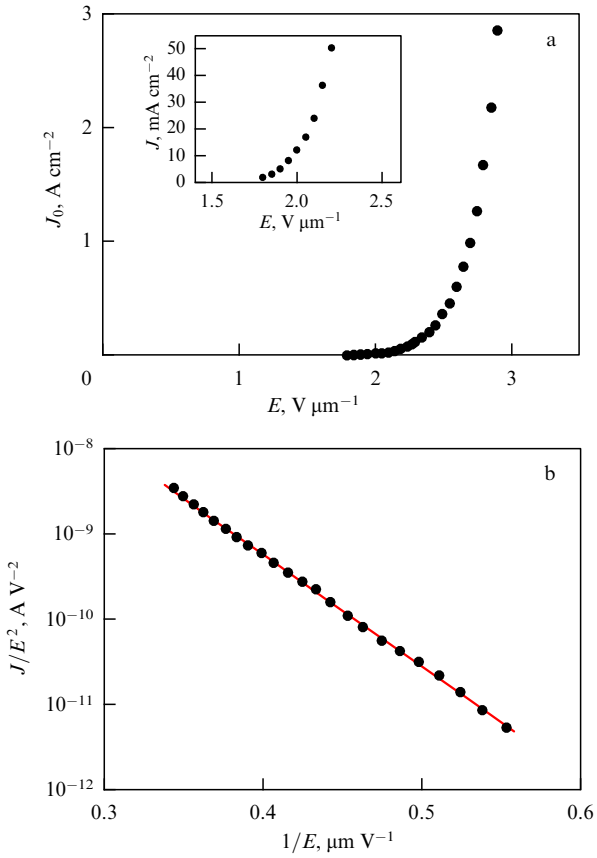

Figure 12. Emission characteristics of a bundle of aligned nanotubes: (a) $J-E$ coordinates, and (b) Fowler–Nordheim coordinates [106].

was kept stable for 200 h at the level of 3 μA, which corresponds to the current density of $J = 150$ mA cm^{-2}.

The results of simulations [106] imply an inhomogeneous distribution of the electric field over the edge surface of the bundle. The field strength at the periphery of the bundle cross section notably exceeds that in the central region. Thus, at an applied voltage of 2400 V, corresponding to the average electric field strength of 2.4 V μm^{-1}, the local field in the peripheral region of the edge surface of the bundle amounts to 15 V μm^{-1}, while the value of this parameter in the central region of the cross section equals 4.2 V μm^{-1}. Therefore, the peripheral region of the bundle is the main source of the electron emission, whose contribution determines the high magnitude of the emission current density. Assuming that only those nanotubes making up the outer surface of the bundle contribute to the emission, and estimating from geometric considerations the number of such nanotubes at ≈ 1600, one can estimate that the emission current per nanotube was about 2 nA [106]. This estimate is about three orders of magnitude lower than the emission current limited by thermal instability.

The stability of the emission characteristics of the bundle relating to the ambient atmosphere was studied at a residual oxygen pressure of 5×10^{-7} Torr, an electric field strength of $E = 2.2$ V μm^{-1}, and an emission current density of $J = 30$ mA cm^{-2}. Measurements showed that the emission current decreased to 5% of its initial value after 40 h of operation. However, the emission current was fully recovered upon subsequent vacuum thermal processing at a temperature of 150 °C. This implies the conservation of CNT structure under the oxygen action.

An even higher magnitude of the emission current density was reached by the authors of Ref. [107], who established that homogeneous arrays of vertically aligned CNTs having a high degree of adhesion can be produced as a result of special attention to the surface structure of the substrate. For this purpose, an original procedure of cathode preparation was developed. According to this procedure, called the 'sandwich' method, a cleaned silicon surface is covered with a photoresist layer, which is followed by a standard lithography etching process to form a pattern of holes with a width of 3.5 μm and the distance between two centers of adjacent holes of 10 μm. Then, thin layers of nickel (~ 150 nm), aluminum (~ 2 nm), and iron (~ 2 nm) are successively evaporated onto the patterned photoresist layer. Finally, the residual photoresist is stripped. Afterwards, the Si substrate coated by catalyst arrays is covered by another Si substrate, which is covered by a nonpatterned catalyst stack. This substrate is removed after completing the CNT synthesis procedure. The CNT synthesis was performed in a microwave (MW) plasma reactor operating at a frequency of 2.25 GHz at a power supply of about 1 kW, temperature of 600 °C, and pressure of 25 mbar. A $CH_4 + H_2$ mixture at a ratio of 1 : 9 flowed with a rate of 200 cm^3 s^{-1} (sccm). The gas temperature was maintained by means of an independent MW heater. The emitter samples fabricated were analyzed with scanning and transmission electron microscopes.

The above-described procedure resulted in the fabrication of multiwalled CNT arrays 3.5 × 3.5 μm in size spaced about 10 μm from each other. The nanotubes composing the arrays possess a high degree of homogeneity in height and diameter, which determines good emission characteristics of the emitter. A thin Ni buffer layer between the nanotubes and the substrate provides a robust mechanical connection of the nanotube's base with the substrate material, as well as a good electrical contact. Some improvement in the emission characteristics of the cathode was reached as a result of MW oxygen plasma processing under a bias voltage of −300 V for 3 min. This processing resulted in an increase in the intertube distance in the arrays, which promoted a weakening of the screening effect.

Emission characteristics of the cathode were studied at a residual gas pressure of 8×10^{-9} mbar and interelectrode spacing of 300 μm. At an emission current exceeding 15 mA, the residual gas pressure rose to 5×10^{-7} mbar. A circular tantalum plate 5 mm in diameter was used as an anode. Figure 13 displays the results of measurements. Curve *4* in Fig. 13a relates to the array used without plasma processing. Curves *1–3* present the current–voltage characteristics of the processed arrays measured on various days. Further increase in the anode voltage above 1500 V was accompanied by an abrupt heating and red luminescence of the anode surface. For this reason, high emission current density was obtained for a pulsed mode with a pulse duration of 10 μs and a pulse repetition rate of 100 Hz (the duty cycle of 0.1%).

As can be seen from the dependence depicted in Fig. 13b and related to the pulsed operation mode of the cathode, the emission current density reaches about 3.55 A cm^{-2} at a voltage of 2.89 kV. Taking into account the incomplete coverage of the substrate with CNT arrays (the degree of coverage was 12.25%), the real value of the emission current density reaches 28.9 A cm^{-2}. Measurements indicate that the emission current at the level of 500 mA in the pulse mode keeps its stability for 20 h. Such high indicators are due to the appropriate design of the cathode, providing a high degree of

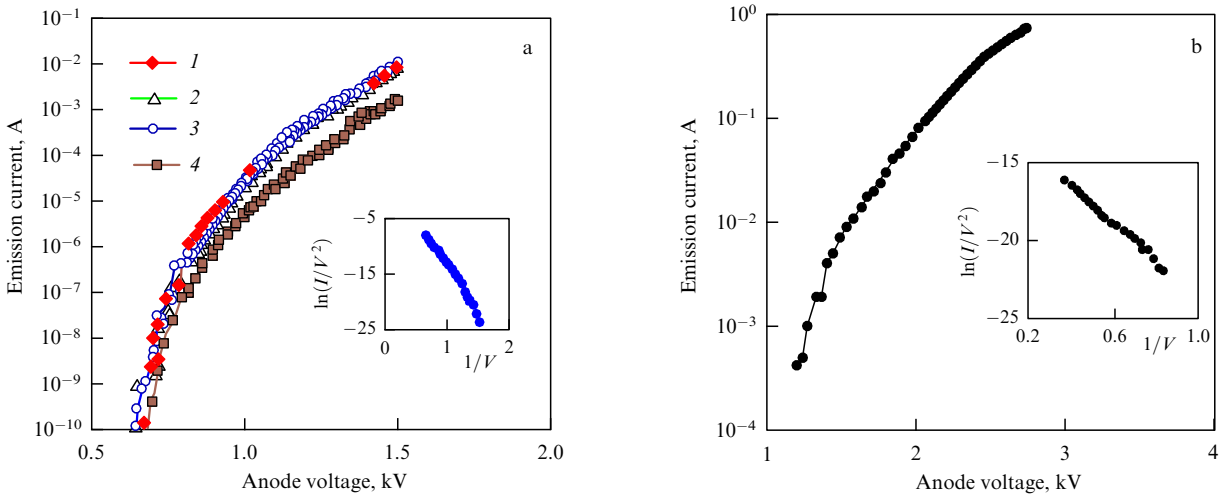

Figure 13. Emission characteristics of multiwalled CNT arrays grown by the 'sandwich' method [107]: (a) cw mode, and (b) pulsed mode.

homogeneity and a good adhesion of carbon nanotubes to the substrate.

The above-described approach to the synthesis of CNT arrays with a high degree of vertical alignment was further advanced in Ref. [108], where the good emission properties of such arrays have been demonstrated. A silicon wafer covered with a diffusion barrier titanium nitride (TiN) layer was used as the substrate to avoid a chemical reaction between the catalyst and the substrate. Then, a nickel film 500 nm thick was evaporated onto the TiN layer. This film acted as a second catalyst layer absorbing CH_x^+ ions and CH_x radicals and forming a buffer interface between the CNTs and the substrate. The Ni layer was covered with the Al layer ~ 2 nm thick preventing the migration and aggregation of catalyst particles. The sandwich thus fabricated underwent to MW plasma processing (2.45 GHz), which was followed by evaporating the Al layer with an Fe layer 2 nm thick acting as a catalyst in the course of CNT growth. The above operational procedure was performed at a residual pressure of 5×10^{-5} mbar and the sample was not exposed to air before being transferred to the CVD chamber.

The nanotubes were grown by applying the MW (2.45 GHz) plasma-assisted CVD method. The discharge power was about 1 kW, the $H_2 + CH_4$ (9 : 1) gas mixture pressure was 25 mbar, and the gas flow rate amounted to 200 cm^3 s^{-1} (sccm). The synthesis was performed at a temperature of 600 °C, which was maintained by means of an MW hydrogen gas discharge heater. While the catalyst was partially oxidized in air, hydrogen plasma processing for 20 min resulted in a reduction of Ni and Fe from oxides.

Scanning and transmission electron microscope observations indicated a high degree of homogeneity in the distribution of emitters over the substrate. The diameter of each emitter consisted of a large number of multiwalled nanotubes measured about 40 μm, while the distance between emitters was 100 μm. The nanotube's height depended on the growth conditions and usually amounted to ~ 6 μm, which corresponds to a growth rate of about 2 μm min^{-1}. The nanotube arrays were subjected to MW oxygen plasma processing, which decreased the density of nanotubes on the substrate, thereby weakening the undesirable screening effect. The processing was performed at a bias voltage of −600 V, MW discharge power of 600 W, residual gas pressure of 4×10^{-4} mbar, and oxygen flowing at 8 cm^3 s^{-1} (sccm). The observations indicated that such a processing did not notably change the vertical alignment of the nanotubes or the degree of their adhesion to the substrate surface, while the density of the nanotubes was considerably decreased.

The emission characteristics of the CNT samples produced were measured in a vacuum chamber in a diode mode at an interelectrode spacing of 250 μm, residual gas pressure of less than 2×10^{-7} mbar, and applied voltage ranging from 0 to 3 kV. A tantalum plate weakly sensitive to electron irradiation was used as an anode. The measurements showed that the threshold magnitude of the gap-averaged electric field strength providing an emission current at the level of 10^{-6} A cm^{-2} was about 3.9 V μm^{-1}. At an anode voltage of 2.8 kV, the emission current reached 20 mA, which corresponds to an emission current density of about 2 A cm^{-2}, taking into account the total cathode surface area of 1 mm^2. Treatment of the current–voltage characteristics provided an evaluation of the electric field amplification factor, which resulted in $\beta = 890$.

One more approach to fabricating a large-area field emitter with high emission current in a pulsed mode has been demonstrated in Refs [110–113]. In this case, multiwalled CNTs about 30 nm in diameter synthesized by the thermal CVD method were used as a source of the emission. Purified CNTs mixed with an organic binder were exposed to ultrasonication for an hour, resulting in the formation of a finely dispersed paste. This paste was applied to a silicon substrate 5 cm in diameter and dried in a nitrogen atmosphere at a temperature of 80 °C for 20 min. Therefore, the film covering the substrate contained nanotubes with a random orientation relating to the substrate surface.

The emission properties of the cathode fabricated were studied in a diode configuration at a residual gas pressure of 10^{-3} Pa in the single-pulse and double-pulse modes [110]. In the case of single pulses, the voltage applied to the interelectrode gap 98 mm in width was ~ 1.64 MV at a pulse duration of ~ 100 ns. In the double-pulse mode, the voltage applied to the gap 65 mm in width was ~ 1 MV, each pulse having a duration of ~ 100 ns and the interval between pulses being 400 ns. The maximum value of the emission current in the single-pulse mode was reached at the gap-averaged electric field strength of 16.7 V μm^{-1} and equaled 1.95 kA,

which corresponds to an emission current density of 99 A cm^{-2}.

In the double-pulse mode, the emission current during the second pulse considerably exceeded that during the first pulse. The maximum emission current was observed at an applied voltage of 1 kV and reached 5.25 kA, which corresponds to an emission current density of 267 A cm^{-2} at a gap-averaged magnitude of the electric field strength of 15.4 V μm^{-1}. A drastic increase in the emission current during the second pulse compared to the first one is caused by formation of a plasma layer near the substrate surface due to the action of the first voltage pulse. The occurrence of the plasma layer changes the distribution of the electric field in the vicinity of the substrate and effectively decreases the interelectrode distance, thus promoting an increase in the electric field strength during the second pulse.

The above approach [110] has been further advanced in Ref. [111], which reports an emission current density of 344 A cm^{-2} at a gap-averaged electric field strength of 16.7 V μm^{-1}. In this case, multiwalled CNTs 30 nm in diameter composed a film 2 μm thick. The film was produced as a result of drying a mixture of purified CNTs (1 g) with an organic solvent (32 g) consisting of ethylcellulose, terpineol, and ethanol in a mass ratio of 1 : 100 : 230. The emission properties of the cathode fabricated were studied in a pulse mode at a residual gas pressure of $\sim 10^{-3}$ Pa. A hollow cylinder 60 cm in diameter was employed as an anode. Two types of the applied voltage pulses were used. In the first case (high-voltage mode), the voltage applied to the interelectrode gap 98 mm in width was $\sim$ 1.64 MV at a pulse duration of $\sim$ 100 ns. In the second case (low-voltage mode), the voltage across the gap 65 mm in width was $\sim$ 0.74 MV at a pulse duration of $\sim$ 100 ns. The time interval between subsequent pulses comprised 120 s, which excluded their influencing each other.

Electron microscope observations indicate that the film surface contains a large number of vertically aligned CNTs 2–3 μm in height spaced about 1 μm from each other. The surface distribution of these nanotubes has a high degree of homogeneity. Some number of the nanotubes can be removed from the film surface by means of adhesive cellophane tape. The visual appearance of the CNT film is notably changed as a result of the emission pulse. Holes appeared on the substrate surface, while part of the vertically aligned nanotubes disappeared. The emission current density decreased as the number of pulses increased. The maximum emission current (6.75 kA) was reached in the first high-voltage pulse at a voltage 1.64 mV applied to the gap 98 mm in width. This corresponds to an emission current density of 344 A cm^{-2} at a gap-averaged electric field strength of 16.7 V μm^{-1}. The cathode is able to stand up to 110 pulses in this mode. In the low-voltage mode, the maximum emission current was reached at an applied voltage of 0.74 MV and equaled 0.98 kA. This corresponds to an emission current density of 50 A cm^{-2} at an average electric field strength of 11.4 V μm^{-1}. In this mode, the cathode stands up to 90 pulses.

Such high values of the emission current in these experiments can be explained by the mechanism of explosive electron emission [114, 115], according to which the electron field emission is promoted by the field amplification phenomenon in the vicinity of the nanotube's tips. Ohmic heating of nanotubes causes a fast transition from electron field emission to the thermionic one which is accompanied by the formation of a plasma layer on the cathode surface. This layer is the main source of electron emission.

4.2 Electron field emission displays

One of the most promising applications of CNT-based electron field emitters relates to the development of displays. Electron field emission displays were first demonstrated tens of years ago utilizing a so-called Spindt configuration [116, 117]. The main advantage of using CNT-based cathodes over those lies in the relatively low supply voltage due to a high value of the electric field amplification factor inherent to nanotubes. In addition, due to the relatively low value of the applied voltage (about 1 kV) devices equipped with CNT-based cathodes operate at short interelectrode gaps, which determines their miniature lateral dimensions and low level of power supply. Because of the high thermal and chemical stability of CNTs, the lifetime of such devices has no core limitations. One more advantage of nanotubes relating to silicon and molybdenum commonly employed in electron field emitters concerns the relative ease of fabrication of such emitters and their mechanical stability. Human sight possesses high sensitivity and is able to respond to a lowering of the operating characteristics of even a single pixel making up an image. Therefore, the lifetime of each single pixel should be no shorter than several years. CNT-based cathodes are able to meet such a strong requirement.

Many research teams have focused their efforts on the development of CNT-based electron field emitters. In particular, the Samsung Corp. has presented a prototype of a 38″ diagonal TV display operating on such a principle [118]. A general approach to the fabrication of a flat display with a CNT-based cathode is described in one of the first publications in the field [119]. In this case, the screen was 1 cm in lateral size. Multiwalled CNTs bound into bundles were synthesized by a standard electric arc method. Then, the soot was dispersed in methanol and annealed in air at 700 °C, which promoted the removal of contaminations, raising the content of the CNTs in the sample up to 80%. Some nanotubes had open ends, while others ended with conical caps with a radius of curvature of about 2 nm.

Figure 14 presents a schematic of the display [119]. A glass plate was used as a cathode. Microtrenches 200 μm in width and 100 μm in depth spaced 300 μm from each other were etched on this plate using hydrofluoric acid. Strips of epoxy resin containing up to 50 vol. % CNTs were inserted into the trenches. The surface density of the CNTs was about 2 μm^{-2}. A similar glass plate filled with phosphor strips 200 μm in

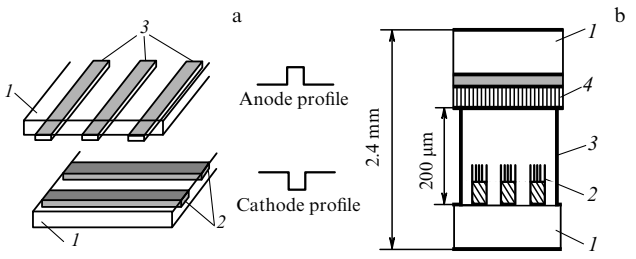

Figure 14. Schematic representation of flat displays with CNT-based cathodes: (a) progenitor model [119]: *1* — glass plates; *2* — epoxy resin strips containing CNTs; *3* — phosphor strips. (b) Color display 132 × 113 × 2.4 mm in size [120]: *1* — glass plates 1.1 mm thick; *2* — CNT array at a metal substrate; *3* — separating plates; *4* — phosphor matrix.

width and 300 μm in length was used as an anode. The inter-electrode spacing was kept at the level of 30 μm. The CNT strips were arranged perpendicular to those of the phosphor, resulting in the formation of individual pixels at their intersections. The total number of such pixels at the emitter 1×1 cm in area amounted to 16. The emission current–voltage characteristics measured for each pixel independently at a residual gas pressure of 10^{-6} Torr were superimposed on each other with a high accuracy. This implies a high degree of surface homogeneity of the emitter. The instant emission current density (76 mA mm^{-2}) of the pixels required to drive a diode display was reached at a voltage of 230 V. The measured current fluctuation level at a voltage of 300 V did not exceed 8% over 12 h. A legible image of a letter consisting of 12 pixels was displayed.

The design and practical testing of a 4.5-inch full-color display was the next step on the road to developing flat panel displays with CNT-based cathodes [120]. This device, depicted schematically in Fig. 14b, contains two glass plates 1.1 mm thick, one of which is coated with a patterned layer of single-walled nanotubes, and the second coated with a phosphor layer. The separation between the substrates was kept at 200 μm. Single-walled carbon nanotubes about 1.4 nm in diameter and 0.5–2.0 μm in length were produced in an electric arc with graphite electrodes using the standard method, which was followed by purification with a 1 : 1 mixture of nitric and sulphuric acids at $T \sim 1000\,^{\circ}$C. The purified samples containing CNTs were cut into small pieces, washed with distilled water, dried, and then ultrasonicated in isopropyl alcohol. This resulted in the formation of a finely dispersed suspension which was mixed with an ultradispersed metal powder and an organic binder. The mixture obtained was applied over the substrate; the binder was then removed through thermal treatment at $T \sim 300\,^{\circ}$C for 20 min. Metal particles were next removed from the cathode surface using a surface rubbing process, causing some CNTs to protrude from the top surface. The anode surface was coated with a phosphor layer involving Y_2O_2S : Eu, ZnS : Cu, Al and ZnS : Ag, Cl 6–10 μm thick, corresponding to the red, green, and blue colors, respectively. After thoroughly establishing the separation between the substrates, the display panel was pumped out down to a pressure of 10^{-7} Torr and sealed off at $T \sim 415\,^{\circ}$C in a medium of highly purified Ar. The display manufacturing procedure is easily reproducible and scalable.

The monitor produced in such a manner was utilized to display a color image with a high degree of surface homogeneity and time stability. It was tested using green phosphor at an anode voltage of 800 V, which corresponded to an electric field strength of 4 V μm^{-1}, a duty ratio of 1/4, and a frequency of 15.7 kHz. A brightness of 1800 cd m^{-2} was achieved in the above conditions. Such high operating parameters of the display stem from the high degree of vertical alignment of CNTs on the cathode surface, their considerable surface density, and the good surface homogeneity of the cathode material.

One of the most attractive features of flat panel displays with CNT-based cathodes is the extraordinarily low level of energy consumption, which relates to the low magnitude of the applied voltage. From this viewpoint, a triode scheme appears to be more promising than the above-described diode scheme, because the electron emission current is controlled here with an additional electrode. Such a scheme providing an even lower level of power consumption has been realized in the recent publication [121]. In this work, single-walled nanotubes were produced by the standard electric arc method in a helium atmosphere. One gram of the initial soot containing 60 wt. % single-walled CNTs was stirred in 200 ml of a concentrated sulfuric/nitric acid solution of varied composition for several minutes. Then, the suspension obtained was stirred at $100-120\,^{\circ}$C for several hours and filtered by means of a paper filter. The filtered wet powder was washed with distilled water several times and dried at room temperature; thereafter, it was drenched again with distilled water and centrifugated. In order to get a surface charge on the nanotube powder, from 10^{-6} to 10^{-2} mol of $Mg(NO_3)_2 \times 6H_2O$ was added to the powder suspension. The electrophoresis coating method was used to deposit carbon nanotubes onto a cathode metal surface. In accordance with the former, a negative dc bias of 10–50 V was applied to the cathode, which resulted in selective deposition of nanotubes on the patterned electrode surface. As follows from scanning and transmission electron microscope observations, Raman spectral measurements, and thermogravimetry analysis, the nanotubes obtained are bound into bundles 10–30 nm in diameter and do not contain metal contaminants.

As follows from numerical calculations, the electric field amplification effect strongly disturbs the homogeneity of the electron emission from the end surface of a bundle. Therefore, the current density emitted from a peripheric site of the surface considerably exceeds that for a middle region. In order to avoid this phenomenon, a gate electrode was incorporated between cathode and anode, which results in the triode configuration [122] presented schematically in Fig. 15. The gate electrode separated by 1.1 mm from the cathode has a set of holes 300 μm in diameter, providing the passage of emitted electrons. A green-light-emitting phosphor ZnS : Cu, Al was utilized for characterization of the field emission. The gate bias varied between 100 and 300 V following a sine law on a frequency of 25 kHz. The luminescence brightness of the phosphor was determined by the anode voltage. Thus, a brightness of 1000 cd m^{-2} was achieved at a gate voltage of 220 V, and an anode voltage of 900 V. The screen luminescence is characterized by a high degree of surface homogeneity and time stability. The fluctuation level of the brightness at a pressure of 5×10^{-6} Torr in the chamber did not exceed 5% over 12 h. Usage of the triode configuration opens the way to resolving the technical problems arising in the development of displays with CNT-based cathodes. One such problem relates to the accumulation of a charge on the plates separating the cathode and the anode. Another problem lies in the necessity of keeping relatively high potential difference between the electrodes separated by a rather short distance. This feature, caused by the emission properties of the cathode and the

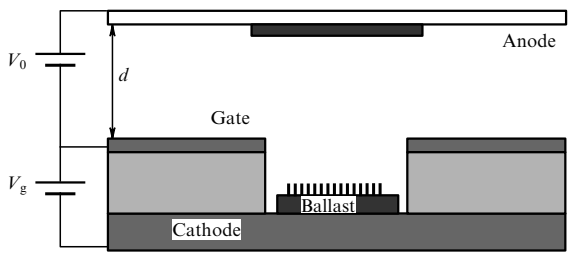

Figure 15. Triode scheme of control for a pixel, containing a ballast resistance connected in series with the emitter [122].

effectiveness of the phosphor, complicates the design of the device and increases its cost. The presence of the third electrode allows the control of the emission by fitting the voltage between the cathode and the grid within a range of several volts. The acceleration of electrons up to the final energy occurs in a gap between the grid and the anode.

The control electrode promotes focusing of the electron beam, which enhances the brightness and the contrast of the image. In an ideal situation, the electron beam emitted by a specified cathode pixel should reach a particular anode pixel. However, this ideal picture is usually disturbed due to a spatial spreading of the electron beam emitted by nanotubes of various orientations. A series of publications [123–127] describes displays with CNT-based cathodes equipped with control electrodes that are able to focus the electron beam.

As was considered in Section 3.2, due to the natural statistical spread of the geometric characteristics of nanotubes engaged in a specific pixel, only a small part of the nanotubes contributes to the emission current of the pixel. For this reason, nanotubes belonging to this part primarily undergo degradation. These nanotubes are distinguished from surrounding neighbors by an increased height and smaller diameter. To suppress this phenomenon, the emission current of nanotubes can be limited by inserting a ballast resistance into the emitter's power supply circuit. Due to such a limitation, a rise in the emission current is accompanied by a lowering of the applied voltage, thus preserving individual emitters from quick thermal decomposition and also providing a higher degree of spatial homogeneity of the emission. One more way to avoid the thermal degradation of emitters consists in division of a pixel into smaller subpixels possessing an independent electronic control. Further opportunities in this area relate to the usage of CNTs of enhanced length, which are able to clean themselves as a result of self-heating, and utilizing systems gaining an electronic signal [128].

4.3 Lighting lamps based on the electron field emission of CNTs

One of the first areas of application of CNT-based cathodes relates to the development of lighting lamps. In this case, the electrons emitted by the cathode and accelerated in the interelectrode gap hit the phosphor where their energy transforms into light. The design simplicity of such a light source and quite high coefficient of transformation of the input energy into light have attracted considerable interest in the problem from researchers and developers [129–133]. The most advanced commercial device developed at the initial stage of research was described in Ref. [129]. The first version of such a device was similar in its construction to the well-known cathode ray tube where the upper surface of a cylinder serves as a source of radiation. Such sources have been under development since 1998 and at present they are being employed in commercial devices [130]. Usually, such devices employ thermionic cathodes possessing high emission characteristics. However, the cathode in these devices must be heated up to several hundred degrees centigrade, which complicates the construction of the lamp and increases power consumption. These drawbacks are obviated through the usage of CNT-based field emission cathodes. As an example of the appropriate realization of such an approach can be mentioned Ref. [129] reporting an effective light source with a cathode based on multiwalled CNTs, which holds stable characteristics for up to 10,000 hours.

In this work [129] multiwalled CNTs were synthesized in a standard electric arc with graphite electrodes at an He pressure of 200–500 Torr, discharge current of 50–70 A, and applied voltage of about 25 V. The anode rod was 6 mm in diameter, while the cathode rod was 13 mm. The material containing nanotubes had the form of a disk 0.5–1 mm thick and 6 mm in diameter and was extracted from the inner part of the cathode deposit; it was attached to a stainless steel plate $5 \times 5 \times 0.15$ mm in size by means of a silver-based cement. The material was annealed at a temperature of 450–500 °C to remove hard contaminations. As a result, only a fibrous kernel 2–3 mm in diameter consisting mainly of nanotubes remained on the disk. The cathode thus fabricated was inserted into a cathode ray tube instead of a standard thermionic cathode. The electron field emission of this cathode was controlled by means of an additional grid electrode spaced 0.5–1 mm from the cathode surface. Aluminum foil 100–150 nm thick applied to a glass substrate and covered with a phosphor layer was utilized as an anode. The lamp was evaluated down to a residual gas pressure of 10^{-8} Torr. The cathode was grounded and the voltage applied to the grid ranged between 0.6 and 1.2 kV. The anode voltage was usually 10 kV. The measurements performed indicate that about 60% of emitted electrons pass through the grid and reach the anode surface. The fluctuation level of the emission current did not exceed 4% over 10 min. The brightness of the anode luminescence was measured at an anode current of 200 mA by using color phosphors ZnS:Cu, Al (green); Y_2O_3:Eu (red) and ZnS:Ag (blue), which resulted in values of 6.3×10^4, 2.3×10^4, and 1.5×10^4 cd m^{-2}, respectively. This is about double the amount of the characteristic brightness of commercial light sources operating on the basis of thermionic cathodes at a current of 100 mA. These parameters of the lamp are high enough for use in outdoor illumination systems.

The construction of the cathode-ray lighting lamp was improved considerably in Ref. [134], where, in contrast to traditional systems of such a kind, the light was emitted from the cylindrical, but not from the end, surface of a glass tube. A wire 1 mm in diameter and 7 cm in length fabricated from an Fe/Al/Cr alloy was used as a substrate for the CNT emitter. The wire was moistened with a water $Fe(NO_3)_3 \times 9H_2O$ solution containing iron particles used as a catalyst. The nanotubes were grown by the CVD method on the surface of the wire inserted into a cylindrical quartz reactor 12 mm in diameter under a flow of acetylene (20 ml min^{-1}) and nitrogen (80 ml min^{-1}) at a temperature of 720 °C and atmospheric pressure. The synthesis procedure resulted in the formation of bent multiwalled CNTs about 20 nm in diameter on the cylindrical surface of a substrate. The emission properties of the cathode were studied in a vacuum chamber at a residual gas pressure of 10^{-7} Torr with the employment of a cylindrical aluminum anode 42 mm in diameter and 5 cm in length. The current–voltage characteristics of the emitter measured at an applied voltage of up to 500 V fit well with the classical Fowler–Nordheim dependence. The emission current density of 1 mA cm^{-2} is reached at an applied voltage of 1.1 kV. Such a high result can be explained in part by the usage of a cylindrical geometry of the electrodes, due to which the electric field strength in the vicinity of the cathode exceeded the corresponding quantity occurring in the case of a flat geometry of the gap by the factor $\ln(r_2/r_1)$ (here, r_1 and r_2 are the radii of the cathode and anode, respectively). Processing the current–voltage characteristics, assuming

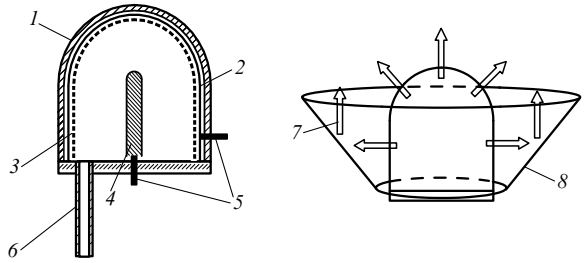

Figure 16. Schematic representation of the construction of a cathode-ray lighting lamp [134]: *1* — glass retort, *2* — anode in the form of a transparent conducting ITO film, *3* — phosphor layer, *4* — nanocarbon cathode, *5* — electrodes, *6* — glass pipe for sealing off the lamp, *7* — direction of the light emitted by the phosphor layer, and *8* — mirror reflector.

that the electron work function for nanotubes equals 5 eV, provided the estimate of the electric field amplification factor: $\beta \approx 23{,}000$.

The emitter fabricated was utilized as a cathode for a luminescent lighting lamp. A cylindrical glass tube, the inner surface of which was covered with a phosphor, served as an anode. At an anode voltage of 5.4 kV, the emission current density reached 0.5 mA cm^{-2}, which corresponds to the anode current density of 0.06 mA cm^{-2}. Under these conditions, the luminescence brightness amounted to 10,000 cd m^{-2}, which is comparable to the relevant magnitude for commercial sources. However, as distinct from conventional luminescent light sources, the lamp under consideration does not contain ecologically dangerous mercury vapors and is distinctive in ease of switching on and off.

Further efforts aimed at improving cathode-ray light sources with CNT-based cathodes have resulted in the development of a new lamp construction. This construction integrates cylindrical and spherical parts into a common unit [135, 136]. The construction illustrated in Fig. 16 contains a cylindrical cathode with a spherical end covered with a nanocarbon film that works as a source of electron emission. The cathode is inserted into a sealed-off retort, the inner surface of which is covered with an anode conducting transparent film based on tin and indium oxides (ITO) that, in turn, is covered with a phosphor layer. The cathode operates at a residual gas pressure of $10^{-7}-10^{-6}$ Torr. The reflector shown schematically in the right part of Fig. 16 serves to decrease light losses and produce a directional light beam. Measurements performed with a pilot lamp of the above-described construction indicated a luminescence brightness of up to 6×10^4 cd m^{-2}, which is comparable to the best achievements for cathode ray lamps of other types.

4.4 X-ray sources

One more promising field for utilizing CNT-based cathodes relates to the development of portable X-ray sources. Replacing conventional thermionic cathodes with electron field emitters permits obtaining quite high emission current at room temperature and at a moderate level of applied voltage (several dozen kV). Such a substitution results in a considerable enhancement of the lifetime of cathodes and decreases their weight and size, which means a considerable lowering of their cost. What is more, the usage of CNT-based cathodes offers an opportunity to generate sharply focused X-rays that is unattainable with thermionic cathodes. One more important advantage of CNT-based cathodes consists in the short time needed for switching on and off the emission current. This feature permits the development of time-programmed X-ray sources with a time resolution on the nanosecond level, which offers new opportunities for medical and technological applications of devices of this type. It should be noted that the electron field emitters for generating X-ray radiation employ not only CNT-based cathodes but also cathodes based on carbon fibers with a diameter several times larger than that of multiwalled CNTs [137].

One of the first constructions of an X-ray source with a CNT-based cathode was described by the authors of Ref. [138], who used a three-electrode configuration to control the emission current. In this construction, a single-walled CNT film was applied by the electrophoresis method onto a flat metallic disc substrate that served as a cathode. The emitter was 0.2 cm^2 in area. Nanotubes about 1.4 nm in diameter were bound into bundles about 50 nm in diameter.

To generate the emission current, a controllable voltage of several hundred volts was applied to an additional electrode comprising a metal grid spaced from the cathode surface by 50–200 μm. Electron emission was observed at a residual gas pressure of 5×10^{-7} Torr. X-ray radiation was generated by means of a copper plate target. The experiments were conducted in the pulse mode at a pulse repetition rate of 30 kHz.

The possibility of generating X-ray radiation with a high degree of time and spatial resolutions is important for the development of X-ray sources designed for producing images of fast-moving complex-shaped objects. The subsequent processing of such images forms the basis of X-ray computer tomography. Conventional X-ray scanners used for this task record a set of sequential images of a moving object, which requires quite intense X-ray radiation and limits the development of such systems. This problem is resolved by using multipixel CNT-based emitters [26] (see also Ref. [29]) permitting the time and spatial modulations of the X-ray beam. Such an approach allows one to treat simultaneously the images obtained from different pixels composing the cathode, resulting in a drastic increase in the maximum attainable velocity of a moving object without enhancing radiation intensity and without sacrificing image quality.

A multipixel X-ray source is shown schematically in Fig. 17a (on the right). This device, operating at a residual gas pressure of 10^{-8} Torr, contains an array of nine CNT-based cathodes, a common grid, an electrostatic focusing system, and a molybdenum plate target. A thin layer of a composite material containing CNTs is deposited by the electrophoresis method onto a metal substrate served as a cathode. To enhance the stability and spatial homogeneity of the signal, a ballast resistance is connected in series with each pixel, which lowers the level of current fluctuations. Each of 9 pixels provides a focused beam about 200 μm in diameter. The anode voltage is 40 kV, while the grid voltage is adjusted ensuring that the current from each pixel does not exceed 1 mA. X-ray radiation is modulated by means of a programmable set of voltage pulses applied to the grid.

The instrumental resolution of devices for X-ray radiography and tomography depends critically on the possibility of focusing the electron beam onto a micrometer-sized spot. It appears that a CNT-based cathode best meets this requirement due to its ability to emit extraordinarily high electron current density from very small area. The opportunity to generate a thin X-ray beam by means of an electron beam emitted by a CNT-based cathode was specifically demon-

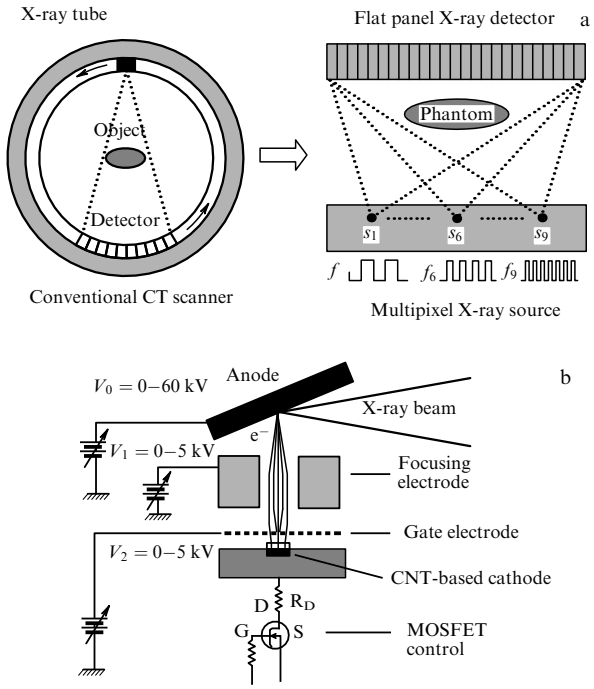

Figure 17. (a) Schematics of the operation of a conventional X-ray scanner (left) and a multipixel X-ray radiation source with a CNT-based cathode (right) [26]. (b) Construction of an individual pixel of the multipixel X-ray radiation source containing a CNT-based cathode, dielectric separating plates 150 μm thick, an additional electrode (grid), and a focusing electrode.

strated by the authors of Ref. [27]. Such an opportunity comes down to the usage of a small-sized cathode providing quite high emission current due to the high emission properties of nanotubes.

The X-ray radiation source consisted of an electron field emission cathode, electrostatic focusing lens, and Cu anode. A bundle of multiwalled nanotubes produced in an He discharge with graphite electrodes served as a source of electron emission. This bundle 0.01–0.1 mm in diameter and about 1 mm in length was attached by means of a conducting paste to the tip of a tungsten wire. As an electrostatic lens, three parallel plates 1 mm thick having central holes 4 mm in diameter were utilized. The first of the plates, playing the role of extracting electrode, was placed directly before the cathode at a distance of 8 mm from its surface. The second plate served as the focusing electrode. The third plate was connected electrically with the first one. These three plates were spaced 4 mm from each other in a symmetrical manner with respect to the focusing electrode. The electrostatic lens described above was placed in the middle between the cathode and anode. An electron beam with a spread angle of 0.19 sr was focused onto a spot several dozen micrometers in diameter on the anode surface. The X-ray beam produced as a result of irradiation of the copper target passed through a Be window spaced 150 mm from the anode surface and was directed to the sample under investigation, which was placed directly on the Be window.

The emission characteristics of the cathode were measured at a residual gas pressure of 5×10^{-7} Torr. The current–voltage characteristic fits well the Fowler–Nordheim dependence within the range of the applied voltage between 1 and 7 kV. At an anode voltage of 7 kV, the emission current equaled 1.3 mA. Measurements performed for 17 h indicate some decrease in the emission current over time, which merged into the saturation. The authors ascribe such a behavior to the shortening of the most protruding nanotubes as a result of thermal destruction and chemical etching. Therefore, CNTs equalize by their length, which is accompanied by the saturation of the time dependence of the emission current. The measured intensity of the focused X-ray radiation reached 0.25 R min^{-1} at an accelerating voltage of 13 kV and emission current of 20 μA. This provided quite sharp images of biological objects, with a resolution better than 30 μm.

One more modification of the multifocus X-ray source with a CNT-based cathode was reported in Refs [139, 140]. In this case, the electron beam emitted by an elliptical-shaped cathode is focused by means of electrostatic lenses. This provides a spot less than 30 μm in diameter on the surface of the molybdenum anode which is also used as an X-ray target. Such a device operates in a triode configuration and its distinctive feature is the inclined orientation of the Mo anode by 9° with respect to the emitter surface. As a source of emission was utilized a homogeneous film of small-diameter multiwalled CNTs deposited onto a highly doped silicon substrate combining the electrophoresis and photolithography methods. The nanotubes were grown by applying the CVD method. After depositing the CNT film by means of cw electrophoresis, the photoresist layer was removed. The region of the cathode surface covered with nanotubes had an elliptical shape 1.0×0.15 mm in size. The focusing system consisted of two flat metal diaphragms and an electrode in the form of a truncated cone which promoted a decrease in the angular divergence of the electron beam after passage of the additional electrode. Thus, the electron beam underwent preliminary focusing before reaching the focusing electrode. Each of the electrodes making up the focusing system was biased independently.

The emission characteristics of the device were measured at a residual gas pressure of about 10^{-7} Torr. The cathode was grounded, while the anode potential run to 40 kV. At a grid voltage providing a gap-averaged electric field strength of 12 V μm^{-1}, the emission current density reached the level of 100 mA cm^{-2}. The percentage of emitted electrons that reached the anode surface came to $\sim 85\%$. The device was tested in both cw and pulsed modes. Measurements indicate that at the pulse repetition rate of 100 Hz and duty ratio of 2% the emission current remains stable at the level of 0.3 mA for 15 h. Scanning the X-ray beam to produce the image of the object under investigation became possible due to the inclined orientation of the target relative to the axis of the electron beam. This permitted the movement of the X-ray beam as a result of displacement of the electron beam by means of the electrostatic focusing system. A single pixel measured 50×50 μm.

One more example of a successful approach to the creation of a similar microfocus electron beam for producing an X-ray beam from a small area of the target surface is reported in Ref. [141]. In this case, the electron beam was focused by an electrostatic lens, whose role was played by an additional electrode (grid), combined with a magnet solenoid.

The microfocus X-ray tube with a CNT-based cathode [141] is shown schematically in Fig. 18a. The device comprises an emitter composed of a sharp tungsten tip covered with nanotubes, an additional electrode (grid), an anode, a magnetic lens based on a solenoid, and a target generating

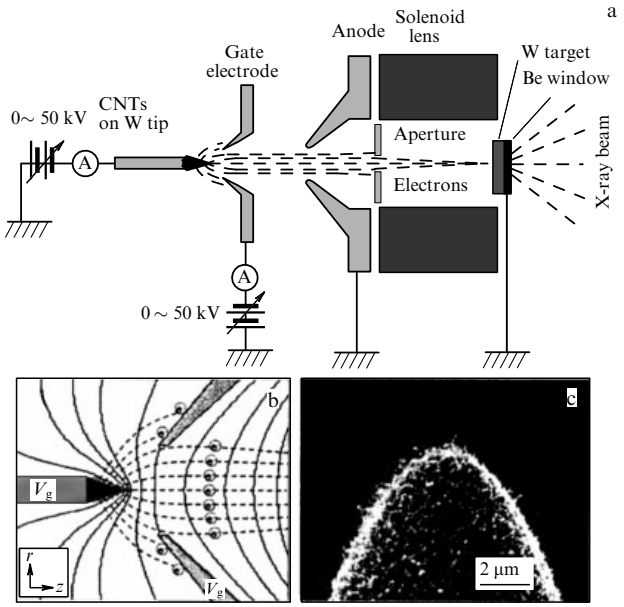

Figure 18. (a) Schematic representation of a multifocus X-ray tube consisting of a CNT-based electron field emitter of the triode type, a solenoid magnetic lens, and a target for the generation of X-ray radiation operating in the transmission mode; (b) the set of electron trajectories calculated for the triode system by means of computer simulation; (c) SEM image of the CNT-based cathode [141].

X-ray radiation and operating in the transmission mode. The electrons emitted by the cathode under the action of the voltage applied to the grid are accelerated by the anode voltage. The additional electrode also acts as a lens, so that the electrons passing through the grid are slightly focused. The final focusing of the electron beam onto a micrometer-sized spot is performed by means of a magnetic lens.

The nanotubes were grown on the surface of a tip 5 μm in radius of curvature that was fabricated from a tungsten wire 250 μm in diameter by the electrochemical etching method. Multiwalled CNTs were synthesized by the plasma-assisted CVD method with the usage of an Ni catalyst. A titanium nitride buffer layer was deposited onto the etched W surface applying the magnetron sputtering method, which improved the adhesion of nanotubes to the substrate. The target utilized for the generation of X-ray radiation was placed close to the solenoid acting as a magnetic lens. A thin metal diaphragm with an aperture ranging between 4 and 10 mm was placed ahead of the lens. A tungsten film 1.1 μm thick applied to a Be window 500 μm thick and 20 mm in diameter was used as a target for generating the X-ray radiation. Under these conditions, the electron mean free path exceeded the thickness of the target.

The current–voltage characteristics of the above-described device were measured at a distance of 0.25 mm between the cathode surface and the grid and a grid voltage of 40 V. The aperture of the diaphragm placed ahead of the focusing lens measured 10 mm in diameter. The threshold value of the electric field strength at the tip, providing the emission current density of 10 mA cm^{-2}, was 1.6 V μm^{-1}, and the electric field amplification factor was estimated as close to 2700. The emission surface area is estimated as 1.6×10^{-6} cm^2, which corresponds to a radius of tip curvature of 5 μm. Measurements indicate that no less than 90% of the emitted electrons reach the target surface. Such a high percentage can be ascribed to a relatively small area of the emitting site in the central region of the hemispherical surface of the tip.

Optimization of the parameters of a microfocus X-ray source with a CNT-based cathode was performed by the authors of Refs [142, 143] through the appropriate combination of computer simulation and direct experiments. This activity resulted in the establishment of quantitative criteria determining the optimum diameter of the X-ray beam and discrimination capacity of the relevant measurements. A film of controllable thickness and morphology containing randomly oriented small-diameter multiwalled CNTs and applied onto a metal substrate by the electrophoresis method was used as a source of the electron emission. A thin tungsten disk with a hole 40 μm in diameter was utilized as an additional extracting electrode. This electrode was separated from the cathode surface by means of a mica plate 150 μm thick. A tungsten disk 1.0 cm in thickness having a central hole 0.6 cm in diameter was placed between the extracting electrode and the anode, being utilized as a focusing electrode. The target surface was oriented at an angle of 6° relative to the emitter surface. Computer simulation provided the following optimum parameters of the system: distance between anode and cathode — 2.5 cm; distance between the grid and the focusing electrode — 0.3 cm; diameter of the cathode site covered with nanotubes — 0.1 cm; grid voltage — 1000 V; focusing electrode voltage — 1000 V, and accelerating anode voltage — 40 kV.

The emission characteristics of the device considered were measured under dynamical vacuum conditions at a residual gas pressure of 10^{-8} Torr. Measurements indicate that electron emission originates at a gap-averaged electric field strength of about 2 V μm^{-1}. The emission current density of 10 mA cm^{-2} is reached at an electric field strength of 2.6 V μm^{-1}. The current–voltage characteristic of the emitter fits the Fowler–Nordheim relation well. Tests performed in the cw mode showed that the emission current remained stable at a level of 0.6 mA for 40 h. This emission current provided an X-ray radiation intensity sufficient for obtaining X-ray images of small animals. In the presence of a ballast resistance, the emission current decreased from 0.61 mA to 0.55 mA over 40 h at the level of short-time fluctuations of 1%. The minimum size of the region emitting X-ray radiation measured 35×35 μm.

The question of developing portable X-ray sources deserves special attention. Such devices, combining portability with a high resolution power, are candidates for use in portable computer tomographs, which can widely spread these effective medical diagnostic devices. One example of such a development has been described in a set of publications [144, 145], where carbon nanofibers were utilized as a source of electron emission. The fibers were grown by the CVD method on the tip of a Pd wire 1 mm in diameter and 2 mm in length that was attached to the end of a tantalum wire by spot welding. After completing the growth process, the Pd wire was safely separated from the tantalum wire for further usage as an electron emitter in the X-ray radiation source.

The X-ray tube 10 mm in diameter was fabricated from a covar alloy. The emitter and the target were inserted inside the tube at a distance of 2 mm from each other. A W rod capped with a hemisphere 2 mm in diameter was used as a target. This rod was half sunk into a copper rod. The Pd wire utilized as a substrate for carbon nanofibers was inserted into a stainless steel tube, so that part of the substrate covered with nanofibers protruded outside. In the device under considera-

tion, the electron beam was self-focused automatically as a result of interaction with the ground wall of the tube. This was also promoted by the open end of the stainless steel tube supporting the Pd substrate. When a voltage of 30 kV was applied to the anode (target), the emission current reached 50 μA, which corresponds to an input power of 1.5 kW.

The emission measurements were performed at a residual gas pressure of 2×10^{-6} Pa. Although the level of short-time fluctuations of the electron current at a fixed target potential reached $\pm(7-8)\%$, the current–voltage characteristics of the emitter barely changed until arcing occurred between the emitter and the target. At a residual gas pressure of about 10^{-6} Pa, notable current fluctuations were nonremovable, independently of the emitter's material, which is due to the influence of residual gases on the emission capability of the cathode. It has been found that the electric arc strikes when the applied voltage builds up too fast. Upon arc termination, the emission current was stabilized in the above-indicated range. Thus, it turned out that arcing destroys only some of the nanofibers, so the emission current is well provided by the remaining fibers that did not undergo decomposition.

Emission current–voltage characteristics measured for a stable current are in good agreement with the classical Fowler–Nordheim dependence. The energy spectrum of the X-ray radiation was recorded by means of a silicon detector placed directly behind a Be window. At a target voltage exceeding 15 kV, the spectrum contained two clearly pronounced tungsten lines L_α and L_β. In this connection, the spectrum did not contain any lines belonging to copper. In spite of a small interelectrode spacing, most of the electrons emitted by the cathode reached the target surface. At a target voltage lower than 10 kV, the X-ray radiation spectrum contained only the continuum caused by electron bremmstrahlung.

It should be noted that the emission characteristics of a carbon nanofiber-based emitter critically depend on such parameters as the size and the shape of the tip, the density of the arrangement of individual fibers at the substrate, fiber length, and the interelectrode distance. It is practically impossible to control all these parameters in the fabrication of the cathode; therefore, the emission characteristics of specific cathodes differ notably from each other. This problem can be partly resolved through the usage of the triode configuration permitting the compensation of the spread in the emission capability of various emitters by applying a controllable voltage to the additional electrode. However, this modification occurs at the expense of an increase in the weight and size of the X-ray source, and the relevant increase in its cost.

The stability of the operating parameters of a carbon nanofiber-based emitter is limited by the processes of sputtering of the cathode surface by positive ions that form as a result of the electron impact ionization of the residual gas molecules. This leads to the formation of atomic-sized inhomogeneities on the surface of the emitter, promoting the amplification of the electric field and increasing the degree of inhomogeneity of the emission current. Thus, the regions of the emitter on which the higher electric field is concentrated are more exposed to heating and show a trend toward melting and thermal decomposition.

4.5 Traveling wave lamps and microwave amplifiers

Satellite communication systems play an important role in the development of modern telecommunication networks, because they are able to satisfy practically all of society's demands for telephonic communications and TV broadcasting. However, the possibility of utilizing such systems on satellites is limited by the considerable mass and size of traveling wave lamps and MW radiation amplifiers that form their basis [146]. One of the effective approaches to lowering these parameters includes the replacement of conventionally used thermionic cathodes with CNT-based electron field emission cathodes possessing considerably lower weight and size. In this case, the advantage of using a CNT-based electron field emitter lies not only in the small size and input energy but also in the very short response time of such emitters. This offers a relatively easy opportunity to modulate the emission current at frequencies on the order of tens of GHz within the framework of triode configuration. In recent years, such a system has been under active development within the framework of a large European project [28, 29, 147–151].

By utilizing CNTs possessing a high electric field amplification factor as a source of electron emission, an additional electrode (grid) can be placed very close to the cathode (10–100 μm). This permits considerably lowering (20–50 times) the electrical capacity of the system and enhancing the maximum reachable value of the modulation frequency.

An electron field emitter could successfully compete with thermionic cathodes if the emission current density reached the level of 1–2 A cm^{-2} [28, 29, 147–151]. In this regard, the total electron current should be no less than several milliamperes, which corresponds to the lateral size of the emitting surface on the level of a fraction of millimeter. The beam electrons are accelerated up to several kiloelectron-volts, so that the total beam power amounts to several dozen watts. This power is enough for the operation of an MW radiation amplifier incorporated into a satellite communication system. A typical amplifier of such a kind operating in triode mode is shown schematically in Fig. 19 [147].

The above parameters of a CNT-based cathode can be reached only by using homogeneous arrays of vertically aligned CNTs with an optimum intertube spacing (on the order of their height) as an emission source. In this case, assuming a typical nanotube height of about 1 μm and that the emission current of an individual nanotube, whose magnitude is limited by the development of thermal instability, can reach ≈ 10 μA, the maximum magnitude of the emission current density for a homogeneous array of vertically aligned nanotubes may run to 10 A cm^{-2}.

However, the creation of a homogeneous array of vertically aligned CNTs with a fixed intertube spacing presents a serious technical problem. The authors of the above-cited Refs [28, 29, 147–151] have elaborated a special

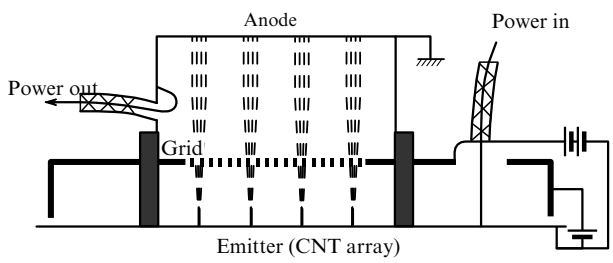

Figure 19. Schematics of a triode type vacuum MW radiation amplifier with a CNT-based cathode [147].

procedure for substrate preparation to solve this problem. In accordance with this procedure, Ni catalyst particles about 100 nm in diameter are applied to a surface of the diffusion barrier titanium nitride (TiN) layer by electron beam lithography. This results in the synthesis of multiwalled CNTs $\sim$ 50 nm in diameter. The synthesis was performed by the plasma-assisted CVD method, providing a high degree of vertical alignment of CNTs in the array due to the straightening action of the electric field. The array of vertically aligned nanotubes 5 μm in height, 50 nm in diameter, and intertube spacing of 10 μm occupied an area of 500 × 500 μm. Therefore, the total number of nanotubes constituting the array was 2500. The total emission current reached 2.5–3 mA in both the cw mode and at a modulation frequency of 1.5 GHz. This corresponds to an emission current density of about 1 A cm^{-2} and the emission current per nanotube at the level of 1 μA. Such high achievements became possible first due to a high degree of homogeneity of the array, providing a roughly similar contribution of most nanotubes to the emission current. Besides that, of great importance is the procedure of thermal treatment of the cathode at a temperature of 850 °C performed at the initial stage of cathode preparation. This procedure promotes lowering the electrical resistance of both the nanotube and CNT/TiN/substrate contact.

In parallel with the triode configuration [147], the diode scheme [28] was also successfully used for MW amplification in the GHz region of the spectrum. In this case, a homogeneous CNT array consisting of 16 individual pixels with above-described characteristics was inserted into a resonator and mounted on the path of an electromagnetic wave. The MW radiation induces an alternative electric field at the nanotube's tips, which promotes electron beam emission with a modulated current density. Therefore, the electromagnetic wave is amplified. The operation frequency of the device is 1.5 GHz. Since the resonator's walls and the cathode are grounded, the MW field occurs only inside the resonator. Tests of the cathode indicated that it operates stably for 40 h at an emission current of 1 mA, showing no evidence of degradation. At a gap-averaged electric MW field strength of 29 V μm^{-1}, the anode current reached 3.2 mA, which corresponds to an average current density of 1.3 A cm^{-2}. The maximum value of current amounted to 30 mA at a current density of 12 A cm^{-2}. Such high magnitudes of the emission current in the GHz frequency range are reachable due to the usage of a CNT-based electron field emission cathode.

Raising the frequency of the electromagnetic radiation that can be amplified by means of vacuum field emission amplifiers with CNT-based cathodes became possible due to a decrease in the interelectrode distance in such devices. This allows lowering the electrical capacity of the interelectrode gap, which promotes a shortening of the response time and an increase in the operation frequency of the device. Unlike metal-based electron field emitters, CNT-based emitters possess higher thermal stability, promoting the generation of higher emission currents without the risk of thermal decomposition of the cathode.

MW radiation amplifiers based on traveling wave tubes with CNT cathodes are being developed and modified in many laboratories around the world. In this connection, there should be mentioned an original triode system of focusing an electron beam, as described in Refs [152–154] and presented schematically in Fig. 20. The distinctive

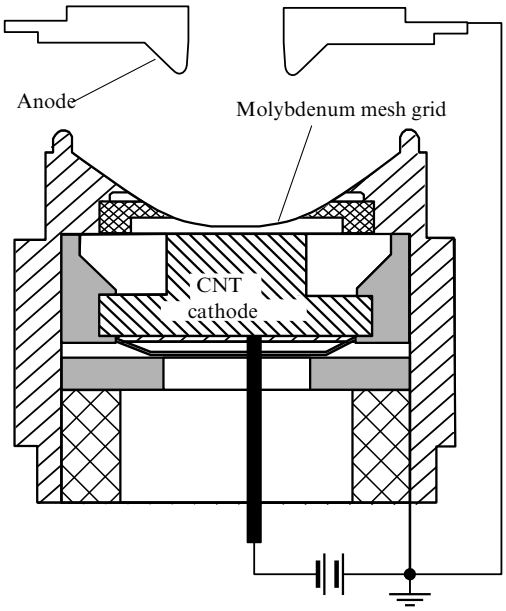

Figure 20. Schematic of a traveling wave lamp with a CNT-based cathode [154].

feature of this construction is the small distance (200 μm) between the cathode and molybdenum grid, providing operation in the gigahertz frequency range. The grid is 38 μm thick and the holes are 216 × 216 μm in size. The measured value of the electron transmission coefficient for the grid is 72%. The interelectrode distance measures 4.5 mm. A paste containing multiwalled nanotubes and an inorganic binder was used as a source of electron emission. This paste was applied onto a hemispherical surface of a cathode having a radius of curvature equaled to 9.73 mm.

The emission properties of the device under consideration were measured at a vacuum level with the residual gas pressure of about 10^{-7} Torr. Measurements indicate that an emission current of 2 mA is reached at an electric field strength of 4.2 V μm^{-1} in the vicinity of the emitter's surface. At low values of applied voltage, the current–voltage characteristic of the emitter agrees well with the Fowler–Nordheim dependence. However, the rise in the applied voltage results in a deviation from this dependence, which manifests itself in the saturation of the emission current. A further increase in the applied voltage is accompanied by a rise in the emission current according to the Fowler–Nordheim equation. However, the magnitude of the electric field amplification factor restored from the experimental current–voltage characteristic and evaluated on the basis of this dependence turned out to be different from that observed at low fields. Such a behavior of the emission characteristics is ascribed to the above-mentioned effect of the formation and desorption of adsorbates on the surface of nanotubes (see Section 2.4).

It should be noted that the maximum current density emitted by the cathodes in MW radiation amplifiers can be quite high, amounting to about 10 A cm^{-2}, in agreement with the above estimates. This is reached through the appropriate choice of parameters characterizing the geometry of an array. The series of publications [155–158] describe in detail a procedure for optimizing the geometric parameters of a CNT array, resulting in the creation of a cathode that is able

to operate at gigahertz frequencies and an emission current density of up to 10 A cm^{-2}.

The CNTs were synthesized on a silicon substrate covered with an SiO_2 layer 400 nm thick under the flow of C_2H_4 (380 cm^3 min^{-1}) and H_2 (190 cm^3 min^{-1}) at a total pressure of 200 Torr and a temperature of 650 °C for 15 min. An Fe film 10 nm thick patterned onto the substrate by electron beam lithography was used as a catalyst. The substrate prepared in such a manner was inserted into a quartz tube 5 cm in diameter, which was placed into a furnace. The nanotubes were grown only on the sites covered with the Fe catalyst. These sites were shaped like circles 0.2–5 μm in diameter spaced 2–100 μm from each other and composed arrays ranging from 500 μm up to several millimeters in size. It was found that the nanotubes grown on the catalyst sites exceeding 0.5 μm in diameter and spaced apart by more than 2 μm were bound into bundles, while the nanotubes grown on catalyst sites of smaller sizes formed a structure somewhat similar to forest debris.

The optimum geometry of the emitter providing the maximum emission current density was evaluated on the basis of comparative measurements of the emission current–voltage characteristics of cathodes differing from each other by the bundle sizes and interbundle distances. In these measurements, a tungsten probe with a flat circular cap 100 μm in diameter was used as an anode. The interelectrode distance was held at the level of 15 μm by means of a micrometer. Emitters with various bundle geometries were fixed on the surface of a flat ceramic stage and were inserted into a vacuum chamber. In this case, an area of the surface site contributing to the emission current corresponded to the anode surface area. Emission characteristics were measured at a residual gas pressure of $(1-7) \times 10^{-5}$ Pa.

The measurements showed that the highest emission current density was reached for an array of vertically aligned bundles ~ 20 μm in height and 1 μm in diameter, spaced apart by 5 μm. Each of such bundles contained up to several thousand individual multilayer CNTs 10–20 nm in diameter. In this case, at an electric field strength of about 10 V μm^{-1} in the vicinity of the emitter's surface, the current emitted from an array 10^{-4} cm^2 in area reached about 1 mA, which corresponded to an emission current density exceeding 10 A cm^{-2} [155–158].

5. Conclusions

The discovery of carbon nanotubes is one of the most considerable achievements of modern science. This carbon modification is intermediate in structure between graphite and fullerenes. However, with respect to many properties carbon nanotubes have nothing in common with either graphite or fullerenes. This permits one to consider and study nanotubes as a proper material possessing unique physical and chemical characteristics.

Carbon nanotubes, like fullerenes, were discovered as a result of purely basic studies addressed at establishing the origin and structural peculiarities of carbon clusters forming as the result of thermal decomposition of graphite. However, shortly after the discovery of nanotubes it was found that the extraordinary physical and chemical properties of these objects offer possibilities for a wide variety of applications. Specifically, good conductivity combined with miniature sizes make nanotubes a unique source of electron field emission. The usage of nanotubes as emitters in electron field cathodes permits a considerable improvement in the operational characteristics of such devices as flat panel displays, cathode-ray luminescent lighting lamps, X-ray tubes, MW radiation amplifiers, and so on. Vacuum devices with CNT-based cathodes are distinguished by a high degree of long-term stability, reduced size, weight, and power consumption level. Therefore, one can note the appearance of a new field of vacuum electronics based on the usage of CNT-based electron field cathodes. Analysis of a huge number of publications directed at the investigation and the optimization of emission characteristics of such cathodes suggests that the relevant devices whose first progenitors have been recently designed and tested will receive wide acceptance in the nearest future.

Researchers studying the physical and chemical properties of carbon nanotubes and exploring the possibilities of their practical application have traveled a considerable way during the 20 years which have passed since their discovery. The following issues can be noted as important stages characterizing this progress: the discovery of multiwalled [2] and, subsequently, single-walled [159] nanotubes; the discovery of the capillarity phenomenon and the ability to fill nanotubes with liquid substances [160]; the establishment of an interconnection between the structural and electronic characteristics of a single-walled nanotube [161]; the elaboration of the method for producing CNTs on the basis of thermal catalytic decomposition of hydrocarbons [162]; the discovery of electron field emission from nanotubes [14–20]; the elaboration of a method for the large-scale production of single-walled nanotubes with close structural and electronic characteristics [51]; the discovery of 2D crystals consisting of single-walled CNTs [163]; the development of methods for the homogeneous patterned filling of large-area surfaces with similarly aligned nanotubes having close electronic characteristics [164–166], and the manufacture of a model sample of a flat panel display with a CNT-based field emission cathode [118]. This list of achievements in the field can be easily continued; however, it is already obvious that during a short period of time we have seen a passage from the description of elongated objects, formed as a result of the thermal decomposition of graphite, through the synthesis of nanotubes with prescribed structural and electronic characteristics, to the fabrication of reliably operating CNT-based cathodes. This example shows again the important fruitful role of basic research, which can result in the quick progress of applied technologies upon the successful concurrence of circumstances.

In spite of the above achievements in research and development in the field of CNTs, this material has not yet received appropriate commercial distribution due to several reasons. The solution to the problem of the application of CNTs depends primarily on the production cost of nanotubes in macroscopic quantities, which currently considerably exceeds that of gold. Apparently, such a price excludes the possibility of large-scale applications of this material. Nevertheless, such nanotube properties as their subminiaturized size, extraordinary mechanical strength, record thermal conductivity, good electrical conduction, and high emission characteristics allow one to hope even now for their effective application in such fields as measuring technology, vacuum electronics and nanoelectronics, chemical technology, hydrogen energy, etc. However, advancement in this direction is possible only as a result of the development of relatively cheep methods for producing CNTs with fixed characteristics in

macroscopic quantities. Particularly, in speaking about the development of vacuum electronics with the usage of CNT-based field emitter cathodes, one should conclude that it is necessary to develop methods of growing large-area homogeneous arrays of vertically aligned CNTs of a specific geometry with a well-defined intertube distance. In so doing, a reliable mechanical and electrical contact between nanotubes and the substrate surface should be provided to prevent both mechanical separation of nanotubes from the array and the thermal decomposition of individual emitters due to excessive heating of a nonperfect contact. In spite of the considerable efforts of researchers, such a technology has not yet been developed, hindering the wide distribution of CNT-based emitters. Successfully solving these problems will become one more example of the effective influence of basic research on scientific and technological progress.

The author cordially thanks L A Chernozatonskii for reading the manuscript and numerous helpful remarks promoting improvement of the text. This work was partially supported by grant No. 436 RUS 113/990/0-1 within the framework of the Agreement on Scientific Collaboration between Deutsche Forschungsgemeinschaft and the Russian Academy of Sciences, and also by RFBR grant No. 10-08-00623-a.

References

1. Eletskii A V *Usp. Fiz. Nauk* **172** 401 (2002) [*Phys. Usp.* **45** 369 (2002)]
2. Iijima S *Nature* **354** 56 (1991)
3. Radushkevich L V, Lushkinovich B M *Zh. Fiz. Khim.* **26** 88 (1952)
4. Endo M, Koyama T, Hishiyama Y *Jpn. J. Appl. Phys.* **15** 2073 (1976)
5. Oberlin A, Endo M, Koyama T *Carbon* **14** 133 (1976)
6. Eletskii A V *Usp. Fiz. Nauk* **174** 1191 (2004) [*Phys. Usp.* **47** 1119 (2004)]
7. Eletskii A V *Usp. Fiz. Nauk* **177** 233 (2007) [*Phys. Usp.* **50** 225 (2007)]
8. Saito R, Dresselhaus G, Dresselhaus M S *Physical Properties of Carbon Nanotubes* (London: Imperial College Press, 1998)
9. Dresselhaus M S, Dresselhaus G, Avouris P (Eds) *Carbon Nanotubes: Synthesis, Structure, Properties and Applications* (Berlin: Springer, 2001)
10. Loiseau A et al. (Eds) *Understanding Carbon Nanotubes: From Basics to Applications* (Berlin: Springer, 2005)
11. Rotkin S V, Subramoney S (Eds) *Applied Physics of Carbon Nanotubes: Fundamentals of Theory, Optics and Transport Devices* (Berlin: Springer, 2005)
12. Ebbesen T W (Ed.) *Carbon Nanotubes: Preparation and Properties* (Boca Raton, Fl.: CRC Press, 1997)
13. Eletskii A V *Usp. Fiz. Nauk* **179** 225 (2009) [*Phys. Usp.* **52** 209 (2009)]
14. Gulyaev Yu V et al., in *IV MC'94: 7th Intern. Vacuum Microelectronics Conf., Grenoble, 1994* (*Technical Digest*) (Piscataway, NJ: IEEE, 1994) p. 322
15. Gulyaev Yu V et al. *J. Vacuum Sci. Technol. B* **13** 435 (1995)
16. Chernozatonskii L A et al. *J. Vacuum Sci. Technol. B* **14** 2080 (1996)
17. Chernozatonskii L A et al. *Chem. Phys. Lett.* **233** 63 (1995)
18. Gulyaev Yu V et al. *Mikroelektronika* **26** (2) 84 (1997) [*Russ. Microelectronics* **26** 66 (1997)]
19. De Heer W A, Châtelain A, Ugarte D *Science* **270** 1179 (1995)
20. Rinzler A G et al. *Science* **269** 1550 (1995)
21. Sohn J I et al. *Appl. Phys. Lett.* **78** 901 (2001)
22. Wang Q H, Yan M, Chang R P H *Appl. Phys. Lett.* **78** 1294 (2001)
23. Mauger M, Binh V T *J. Vac. Sci. Technol. B* **24** 997 (2006)
24. Saito Y, Uemura S *Carbon* **38** 169 (2000)
25. Yue G Z et al. *Appl. Phys. Lett.* **81** 355 (2002)
26. Zhang J et al. *Appl. Phys. Lett.* **89** 064106 (2006)
27. Kawakita K et al. *J. Vac. Sci. Technol. B* **24** 950 (2006)
28. Teo K B K et al. *Nature* **437** 968 (2005)
29. Milne W I et al. *J. Vac. Sci. Technol. B* **24** 345 (2006)
30. Shakir M I et al. *Nanotechnology* **17** (6) R41 (2006)
31. De Jonge N, Bonard J-M *Proc. R. Soc. London A* **362** 2239 (2004)
32. Cheng Y, Zhou O *C.R. Physique* **4** 1021 (2003)
33. Fowler R H, Nordheim L *Proc. R. Soc. London A* **119** 173 (1928)
34. Gomer R *Field Emission and Field Ionization* 2nd ed. (New York: AIP, 1993)
35. Dobretsov L N, Gomoyunova M V *Emissionnaya Elektronika* (Emission Electronics) (Moscow: Nauka, 1966) [Translated into English (Jerusalem: Israel Program for Scientific Translations, 1971)]
36. Luo J et al. *Phys. Rev. B* **66** 155407 (2002)
37. Han S, Ihm J *Phys. Rev. B* **66** 241402(R) (2002)
38. Qiao L et al. *Diamond Relat. Mater.* **18** 657 (2009)
39. Zheng X et al. *Phys. Rev. Lett.* **92** 106803 (2004)
40. Yaghoobi P, Walus K, Nojeh A *Phys. Rev. B* **80** 115422 (2009)
41. Bulashevich K A, Rotkin V V *Pis'ma Zh. Eksp. Teor. Fiz.* **75** 239 (2002) [*JETP Lett.* **75** 205 (2002)]
42. Mishchenko E G, Raikh M E *Phys. Rev. B* **74** 155410 (2006)
43. Li Z-B, Wang W-L *Chinese Phys. Lett.* **23** 1616 (2006)
44. Sedrakyan T A, Mishchenko E G, Raikh M E *Phys. Rev. B* **73** 245325 (2006)
45. Zhao G et al. *Appl. Phys. Lett.* **89** 193113 (2006)
46. Bocharov G S, Eletskii A V *Zh. Tekh. Fiz.* **75** (7) 126 (2005) [*Tech. Phys.* **50** 944 (2005)]
47. Kokkorakis G C, Modinos A, Xanthakis J P *J. Appl. Phys.* **91** 4580 (2002)
48. Eletskii A V, Bocharov G S *Plasma Sources Sci. Technol.* **18** 034013 (2009)
49. Bel'skii M D et al. *Zh. Tekh. Fiz.* **80** (2) 130 (2010) [*Tech. Phys.* **55** 289 (2010)]
50. Xu Z, Bai X D, Wang E G *Appl. Phys. Lett.* **88** 133107 (2006)
51. Xu Z et al. *Appl. Phys. Lett.* **87** 163106 (2005)
52. Edgcombe C J, Valdrè U *J. Microscopy* **203** 188 (2001)
53. Edgcombe C J, Valdrè U *Philos. Mag. B* **82** 987 (2002)
54. Wei G *Appl. Phys. Lett.* **89** 143111 (2006)
55. Dyke W P, Dolan W W, in *Advances in Electronics and Electron Physics* Vol. 8 (Ed. L Marton) (New York: Academic Press, 1956) p. 90
56. Gadzuk J W, Plummer E W *Rev. Mod. Phys.* **45** 487 (1973)
57. Dean K A, von Allmen P, Chalamala B R *J. Vac. Sci. Technol. B* **17** 1959 (1999)
58. Dean K A, Chalamala B R *J. Appl. Phys.* **85** 3832 (1999)
59. Dean K A, Chalamala B R *Appl. Phys. Lett.* **76** 375 (2000)
60. Dekker C *Phys. Today* **52** (5) 22 (1999)
61. Bocharov G S, Eletskii A V *Zh. Tekh. Fiz.* **77** (4) 107 (2007) [*Tech. Phys.* **52** 498 (2007)]
62. Vincent P et al. *Phys. Rev. B* **66** 075406 (2002)
63. Sveningsson M et al. *Phys. Rev. B* **72** 085429 (2005)
64. Kim P et al. *Phys. Rev. Lett.* **87** 215502 (2001)
65. Yi W et al. *Phys. Rev. B* **59** R9015 (1999)
66. Gao B et al., in *NT'05: 6th Intern. Conf. on the Science and Application of Nanotubes, Gothenburg, Sweden, 2005*, p. 307
67. Huang N Y et al. *Phys. Rev. Lett.* **93** 075501 (2004)
68. Bonard J-M et al. *Ultramicroscopy* **73** 7 (1998)
69. Bonard J-M et al. *Phys. Rev. B* **67** 115406 (2003)
70. Tang H et al. *J. Phys. D* **39** 5280 (2006)
71. Paulini J, Klein T, Simon G *J. Phys. D* **26** 1310 (1993)
72. Wei W et al. *Nano Lett.* **7** 64 (2007)
73. Chai G, Chow L *Carbon* **45** 281 (2007)
74. Chen Y, Shaw D T, Guo L *Appl. Phys. Lett.* **76** 2469 (2000)
75. Konishi Y et al. *Jpn. J. Appl. Phys.* **44** 1648 (2005)
76. Martinson L K, Malov Yu I *Differentsial'nye Uravneniya Matematicheskoi Fiziki* (Differential Equations of Mathematical Physics) (Moscow: Izd. MGTU im. N.E. Baumana, 2002)
77. Vlasova E A, Zarubin V S, Kuvyrkin G N *Matematika v Tekhnicheskom Universitete* (Mathematics in Technical University) Issue 13 *Priblizhennye Metody Matematicheskoi Fiziki* (Approximate Methods of Mathematical Physics) (Moscow: Izd. MGTU im. N.E. Baumana, 2001)
78. Fransen M J, van Rooy Th L, Kruit P *Appl. Surf. Sci.* **146** 312 (1999)
79. Liu X et al. *AIP Conf. Proc.* **544** 288 (2000)
80. Suzuki S et al. *Appl. Phys. Lett.* **76** 4007 (2000)
81. Chen P et al. *Phys. Rev. Lett.* **82** 2548 (1999)
82. Ago H et al. *J. Phys. Chem. B* **103** 8116 (1999)
83. Shiraishi M, Hinokuma K, Ata M *AIP Conf. Proc.* **544** 359 (2000)

84. Bonard J-M et al. *Appl. Phys. Lett.* **73** 918 (1998)
85. Obraztsov A N, Volkov A P, Pavlovskii I Yu *Pis'ma Zh. Eksp. Teor. Fiz.* **68** 56 (1998) [*JETP Lett.* **68** 59 (1998)]
86. Obraztsov A N et al. *Pis'ma Zh. Eksp. Teor. Fiz.* **69** 381 (1999) [*JETP Lett.* **69** 411 (1999)]
87. Obraztsov A N, Volkov A P, Pavlovsky I *Diamond Relat. Mater.* **9** 1190 (2000)
88. Obraztsov A N et al. *Diamond Relat. Mater.* **8** 814 (1999)
89. Obraztsov A N et al. *J. Vac. Sci. Technol. B* **18** 1059 (2000)
90. Obraztsov A N, Pavlovsky I Yu, Volkov A P *J. Vac. Sci. Technol. B* **17** 674 (1999)
91. Chen Z et al. *Nanotechnology* **18** 265702 (2007)
92. Nilsson L et al. *Appl. Phys. Lett.* **76** 2071 (2000)
93. Su W S et al. *J. Appl. Phys.* **106** 014301 (2009)
94. Smith R C, Silva S R P *J. Appl. Phys.* **106** 014314 (2009)
95. Bocharov G S, Eletskii A V, Sommerer T J, in *11th Intern. Conf. on the Science and Application of Nanotubes, Montréal, Canada, June 27 – July 2, 2010*
96. McClain D et al. *J. Phys. Chem. C* **111** 7514 (2007)
97. Seelaboyina R et al. *Nanotechnology* **19** 065605 (2008)
98. Bocharov G S, Eletskii A V, Korshakov A V *Rev. Adv. Mater. Sci.* **5** 371 (2003)
99. Bocharov G S et al. *AIP Conf. Proc.* **723** 528 (2004)
100. Bezmel'nitsyn V N et al. *Fiz. Tverd. Tela* **44** 630 (2002) [*Phys. Solid State* **44** 656 (2002)]
101. Yoshimoto T et al. *Jpn. J. Appl. Phys.* **40** L983 (2001)
102. Matsumoto K et al. *Appl. Phys. Lett.* **78** 539 (2001)
103. Han I T et al. *Appl. Phys. Lett.* **81** 2070 (2002)
104. Wadhawan A et al. *Appl. Phys. Lett.* **79** 1867 (2001)
105. Guillorn M A et al. *J. Vac. Sci. Technol. B* **21** 957 (2003)
106. Fujii S et al. *Appl. Phys. Lett.* **90** 153108 (2007)
107. Chen Z et al. *Nanotechnology* **18** 265702 (2007)
108. Chen Z et al. *Nanotechnology* **18** 095604 (2007)
109. Zhu W et al. *Appl. Phys. Lett.* **75** 873 (1999)
110. Liao Q et al. *Carbon* **45** 1471 (2007)
111. Liao Q et al. *J. Phys. D* **40** 6626 (2007)
112. Liao Q et al. *Appl. Phys. Lett.* **90** 151504 (2007)
113. Liao Q et al. *J. Phys. D* **40** 3456 (2007)
114. Mesyats G A, Proskurovsky D I *Impul'snyi Elektricheskii Razryad v Vakuume* (Pulsed Electrical Discharge in Vacuum) (Novosibirsk: Nauka, 1984) [Translated into English (Berlin: Springer-Verlag, 1989)]
115. Miller R B *J. Appl. Phys.* **84** 3880 (1998)
116. Fursey G *Field Emission in Vacuum Microelectronics* (New York: Kluwer Acad./Plenum Publ., 2005)
117. Spindt C A *J. Appl. Phys.* **39** 3504 (1968)
118. Chen J et al. *Ultramicroscopy* **95** 153 (2003)
119. Wang Q H et al. *Appl. Phys. Lett.* **72** 2912 (1998)
120. Choi W B et al. *Jpn. J. Appl. Phys.* **39** 2560 (2000)
121. Choi W B et al. *Appl. Phys. Lett.* **78** 1547 (2001)
122. Choi W B et al. *Appl. Phys. Lett.* **75** 3129 (1999)
123. Chung D-S et al. *Appl. Phys. Lett.* **80** 4045 (2002)
124. Choi Y S et al. *Appl. Phys. Lett.* **82** 3565 (2003)
125. Jung J E et al. *Physica B* **323** 71 (2002)
126. Yu S G et al. *Appl. Phys. Lett.* **80** 4036 (2002)
127. Chung D-S et al. *Appl. Phys. Lett.* **80** 4045 (2002)
128. Yu S G et al. *Jpn. J. Appl. Phys.* **40** 6088 (2001)
129. Saito Y, Uemura S, Hamaguchi K *Jpn. J. Appl. Phys.* **37** L346 (1998)
130. Saito Y, Uemura S *Carbon* **38** 169 (2000)
131. Obraztsov A N, Kleshch V I *J. Nanoelectron. Optoelectron.* **4** 207 (2009)
132. Croci M et al. *Microelectron. J.* **35** 329 (2004)
133. Antony J, Qiang Y *Nanotechnology* **18** 295703 (2007)
134. Bonard J-M et al. *Appl. Phys. Lett.* **78** 2775 (2001)
135. Obraztsov A N, Kleshch V I "Katodolyuminestsentnaya diodnaya lampa" ("Cathodoluminescent diode lamp"), RF Patent No. 2008141395/09(053681) (Priority data 21.10.2008)
136. Kleshch V I "Avtoelektronnaya emissiya iz nanostrukturirovannykh materialov" ("Electron field emission of nanostructured materials"), PhD Thesis (Moscow: Institute of General Physics, RAS, 2010)
137. Matsumoto T, Mimura H *Appl. Phys. Lett.* **82** 1637 (2003)
138. Yue G Z et al. *Appl. Phys. Lett.* **81** 355 (2002)
139. Cheng Y et al. *Rev. Sci. Instrum.* **75** 3264 (2004)
140. Liu Z et al. *Appl. Phys. Lett.* **89** 103111 (2006)
141. Heo S H, Ihsan A, Cho S O *Appl. Phys. Lett.* **90** 183109 (2007)
142. Zhang J et al. *Rev. Sci. Instrum.* **76** 094301 (2005)
143. Liu Z et al. *Rev. Sci. Instrum.* **77** 054302 (2006)
144. Sugie H et al. *Appl. Phys. Lett.* **78** 2578 (2001)
145. Haga A et al. *Appl. Phys. Lett.* **84** 2208 (2004)
146. Booske J H, Barker R J "Vacuum microwave amplifiers", in *Modern Microwave and Millimeter-Wave Power Electronics* (Eds R J Barker et al.) (Hoboken, NJ: IEEE Press, 2005)
147. Minoux E et al. *Nano Lett.* **5** 2135 (2005)
148. Rupesinghe N L et al. *J. Vac. Sci. Technol. B* **21** 338 (2003)
149. Milne W I et al. *J. Mater. Chem.* **14** 933 (2004)
150. Teo K B K et al. *Nanotechnology* **14** 204 (2003)
151. Chhowalla M et al. *J. Appl. Phys.* **90** 5308 (2001)
152. Han J-H et al. *Diamond Relat. Mater.* **13** 987 (2004)
153. Na Y H, Choi J J, Kim R, in *4th Intern. Vacuum Electronics Conf., IVEC2003*: *Seoul, Korea, 2003* (Piscataway, NJ: IEEE, 2003) p. 88
154. Kim H J et al. *IEEE Trans. Electron Dev.* **53** 2674 (2006)
155. Manohara H M et al. *J. Vac. Sci. Technol. B* **23** 157 (2005)
156. Manohara H M et al., in *38th Lunar and Planetary Science Conf., March 12 – 16, 2007, USA*, p. 1436
157. Manohara H et al. *Proc. SPIE* **5343** 227 (2004)
158. Manohara H M et al. *Nano Lett.* **5** 1469 (2005)
159. Iijima S, Ichihashi T *Nature* **363** 603 (1993)
160. Ajayan P M, Iijima S *Nature* **361** 333 (1993)
161. Saito R et al. *Appl. Phys. Lett.* **60** 2204 (1992)
162. José-Yacamán M et al. *Appl. Phys. Lett.* **62** 657 (1993)
163. Thess A et al. *Science* **273** 483 (1996)
164. Ren Z F et al. *Science* **282** 1105 (1998)
165. Fan S et al. *Science* **283** 512 (1999)
166. Li J et al. *Appl. Phys. Lett.* **75** 367 (1999)